Nuclear speckle fusion via long-range directional motion regulates the number and size of speckles

Authors

Jiah Kim[1], Kyu Young Han[234], Nimish Khanna[5], Taekjip Ha[12367], Andrew S. Belmont[156]

[1]Center for Biophysics and Quantitative Biology, University of Illinois at Urbana-Champaign, Urbana, IL, 61801, USA

[2]Department of Physics, University of Illinois at Urbana-Champaign, Urbana, IL, 61801, USA

[3]Howard Hughes Medical Institute, Baltimore, MD, 21205, USA

[4]CREOL, The College of Optics and Photonics, University of Central Florida, Orlando, FL, 32816, USA

[5]Department of Cell and Developmental Biology, University of Illinois at Urbana-Champaign, Urbana, IL, 61801, USA

[6]Carl R. Woese Institute for Genomic Biology, University of Illinois at Urbana-Champaign, Urbana, IL, 61801, USA

[7]Department of Biophysics and Biophysical Chemistry and Department of Biomedical Engineering, Johns Hopkins University, Baltimore, 21205, MD, USA

Abstract

Although the formation of RNA-protein bodies has been studied intensively, their mobility and how their number and size are regulated are still poorly understood. Here, we show significant increased mobility of nuclear speckles after transcriptional inhibition, including long-range directed motion of one speckle towards another speckle, terminated by speckle fusion, over distances up to 4 um and with velocities between 0.2-1.5 µm/min. Frequently, 3 or even 4 speckles follow very similar paths, with new speckles appearing along the path followed by a preceding speckle. Speckle movements and fusion events contribute to fewer but larger speckles after transcriptional inhibition. These speckle movements are not actin-dependent, but occur within chromatin-depleted channels enriched with small granules containing the speckle-marker protein SON. Our observations suggest a mechanism for long-range, directed nuclear speckle movements, contributing to overall regulation of nuclear speckle number and size as well as overall nuclear organization.

34   ## Introduction

35   Intracellular compartmentalization in eukaryotic cells is thought to represent a key

36   evolutionary advance by which complex biochemical processes can be optimized and regulated

37   within highly crowded cellular environments[1, 2, 3]. Compartmentalization is achieved not only

38   with membrane-bound organelles but also through membrane-less "bodies", including P-bodies

39   and stress granules in the cytoplasm and nucleoli, nuclear speckles, Cajal, and PML bodies in the

40   nucleus. Most membrane-less bodies are RNA-protein-rich complexes which function in

41   transcription, RNA processing, and/or protein modification[4, 5]. Recent studies have led to the

42   concept of RNA-protein bodies forming as the result of a phase transition between constituent

43   RNA and proteins and surrounding cytoplasm or nucleoplasm through a demixing driven by

44   interactions between low complexity sequences and multivalent molecules[6, 7, 8, 9]. RNA-protein

45   bodies have been proven to have general physical characteristics of liquid droplets [4, 5]. For

46   example, P-granules undergo rapid assembly/disassembly, and exhibit dripping, fusion, and

47   wetting by shearing force[10], and nucleoli exhibit viscous fluid dynamics such as liquid bridge

48   formation when they are ruptured[11]. Fluorescence recovery after photobleaching (FRAP)

49   analysis of molecular dynamics showed that RNA-protein bodies continuously turnover many of

50   their constituent molecules over a time-scale from a few seconds to a few minutes[12, 13, 14]. These

51   microscopy observations suggest that these bodies are in a liquid or gel state with a constant flux

52   of constituent molecules.

53   Despite a number of studies examining liquid properties and related behaviors of other

54   cellular bodies, both the physical properties and dynamics of nuclear speckle bodies have not

55   been well studied. Defined originally as interchromatin granule clusters (IGCs) by electron

56   microscopy[15, 16], nuclear speckles contain large clusters of ~20 nm RNP granules and are

3

57   enriched in RNA processing factors and polyadenylated RNAs[17, 18, 19]. Nuclei typically contain

58   20-40 irregular shaped nuclear speckles varying in size from ~0.5 μm to several μm[20].

59   Because "pure" liquid droplet bodies theoretically are predicted to merge into

60   progressively fewer and larger droplets, a major question regarding cell bodies in general is how

61   their number and size are regulated in the cell. Interestingly, with transcriptional inhibition

62   nuclear speckles become rounder and larger with a reduction in their overall number[21, 22]. Live-

63   cell microscopy revealed that normally speckles were relatively stationary, but displayed

64   extension and dissociating particles. However, no peripheral dynamics were observed in the

65   absence of transcription[23]. These previous studies did not address directly whether nuclear

66   speckles also exhibit the general physical properties of RNA-protein bodies or how speckle

67   morphology changes dynamically in terms of speckle numbers, size and shape.

68   Using the change in nuclear speckle morphology induced by transcriptional inhibition as

69   a model system, here we studied the mobility and liquid-like behaviors of nuclear speckles.

70   Consistent with previous observations, we observed a general change in morphology after

71   transcriptional inhibition, with speckles becoming bigger and rounder. This was accompanied by

72   an increase in speckle mobility within the nucleus.

73   Surprisingly this increase in speckle mobility was not random. Instead we observed

74   repeated long-range, directional movement of multiple speckles over similar nuclear trajectories

75   or "tracks" which extended over micrometer distances. These movements ended with fusion of

76   the smaller, mobile speckles with larger, typically stationary speckles. These repeated fusion

77   events contributed to the overall decrease in nuclear speckle number and increased mean speckle

78   size as a function of time after transcriptional inhibition.

79   Perturbing normal actin polymerization did not prevent speckle long-range motion, the

4

80   directionality of this motion, or speckle fusion events. Therefore, we excluded the possibility that

81   actin filaments might provide "tracks" for this speckle movement. Combining live-cell imaging

82   with correlative super-resolution light microscopy revealed speckles move within chromatin-

83   depleted channels. Moreover, paths followed by more than one speckle as visualized by live-cell

84   microscopy contained a concentration of small granules containing the speckle-marker SON

85   within these DNA-depleted channels.

86   Our results are the first demonstration of repeated, long-range directed motion with

87   nucleation and fusion of nuclear speckles in a live cell, revealing a previously unsuspected

88   trafficking mechanism of nuclear speckles likely controlling speckle number and possibly

89   nuclear localization. Overall, our results suggest that the distribution of nuclear speckles is

90   significantly affected by translocation as well as dynamic nucleation and fusion of nuclear

91   speckles, and possibly by changes in nuclear chromatin structure that may remove barriers to

92   long-range speckle movements.

Results

Inhibition of RNA polymerase II transcription changes speckle morphology and increases overall speckle mobility

We used SON protein as a speckle marker to visualize nuclear speckles with high contrast. The SON protein showed the highest concentration in nuclear speckles versus nucleoplasm of any speckle markers we tested, with less distributed diffusely or in foci outside of nuclear speckles than other RS-domain proteins such as SC35 or ASF/SF1[19, 24]. The SON protein contains an RS domain and also 6 other tandem repeat regions unique to SON[25], which may function as a scaffold for protein assembly[25]. The RS-domain is found in a large number of mRNA processing proteins, many enriched in nuclear speckles, as well as some proteins related to RNA pol 2 transcription[26]. Knockdown of SON results in a significant change in nuclear speckle morphology as visualized by immunostaining of SC35, another RS-domain containing speckle-marker protein[25].

Attempts to express SON-EGFP from a cDNA plasmid transgene resulted in variegated and unstable transgene expression. To obtain stable expression, we instead transfected Chinese Hamster Ovary K1 (CHOK1) cells with a BAC transgene containing the full-length SON human genomic sequence engineered by BAC recombineering to express a SON-EGFP fusion protein[24]. Use of this ~200 kb BAC containing large 5' and 3' human genomic sequences flanking the SON gene enabled isolation of stable clones expressing uniform levels of EGFP-SON.

To study dynamics of speckles after transcriptional inhibition, we used 5,6-dichloro-1-β-ribofuranosyl benzimidazole (DRB). DRB blocks transcription via inhibition of kinases involved in transcription elongation[27, 28]. We confirmed in our CHO cell system previous work[21, 22] that large speckles become brighter, rounder, and fewer in number after DRB addition (Fig. 1a, b).

116   The GFP-SON intensity within speckles became ~2.5-fold higher on average 2 hrs after DRB

117   addition. The form factor (FF), defined as $(4*\pi*Area/(Perimeter)^2)$, increased ~50% from 0.50 in

118   control cells to 0.76 on average in DRB treated cells. The FF ranges from 1 for a perfect circle to

119   0 for a line. Transcriptional inhibitors α-amanitin and triptolide (TRL) and the heavy metal

120   cadmium(Cd) had similar effects on speckle morphology as DRB (Supplementary Fig. 1).

121   However, we chose DRB for our imaging studies because it produced less rounding and change

122   in shape of the nucleus in comparison to these other inhibitors. This reduced change in nuclear

123   shape was critical for our tracking of speckle movement using alignment of nuclear images from

124   different time points.

125   Live-cell imaging revealed an obvious increase in nuclear speckle mobility during DRB

126   treatment. (Fig. 1c-e) To facilitate analysis, at each 1minute time point we used 2D projections of

127   3D z-stacks. We used a cross-correlation approach to best correct for nuclear rotations and

128   translations between adjacent time points. In comparison to control cells, in which nuclear

129   speckles showed restricted movements over 1 hour (Fig. 1c, left panel), in DRB-treated cells a

130   significant fraction of nuclear speckles showed longer-range net displacements (Fig. 1c, right

131   panel). Overlapping trajectories corresponded to examples in which nuclear speckles came

132   together and merged (Fig. 1c). DRB treatment increased the mean net displacement, Δd, of

133   nuclear speckles over 1.5 hour from 0.64 to 1.69 μm (p-value = 1.007e-12, paired t-test, Fig. 1d),

134   with the increase of the mean distance change per 1 min time point, from 0.17 to 0.19 μm (p-

135   value=2.2e-16, paired Wilcoxon signed rank test, Fig. 1e).

136

137   **DRB treatment induces long-range, directional speckle movements**

7

138   We characterized movement of individual nuclear speckles after DRB addition by

139   measuring the asymmetry coefficient, AC, together with the net displacement, Δd. We observed

140   speckles for 1.5 hours beginning 30 mins after DRB addition using a 1 min time interval,

141   tracking only those speckles which could be observed in at least 20 consecutive time points. To

142   calculate the AC, we first measured the angle between the directions of speckle displacements

143   for two consecutive time points (Fig. 2a). The AC was then defined as the logarithm to the base 2

144   of the ratio between the frequencies of backward ($180 +/- 30^0$) versus forward ($+/-30^0$)

145   movements over the entire speckle trajectory[29]. Random diffusion produces AC values near 0,

146   since forward motion and backward motion are equally likely. AC values higher than 0 indicate a

147   bias towards forward movements, while AC values below 0 suggest constrained diffusion.

148   To compare speckle mobility in control versus DRB-treated cells, we created a scatter

149   plot summarizing AC values versus net distance displacement for speckles (Fig. 2b). This scatter

150   plot reveals three motion regimes (Fig. 2b, c): Type I trajectories show large net displacements

151   ($\cong 1.25$ μm) with positive AC values as a result of subtrajectories that contain a large number of

152   discrete forward steps. Type II trajectories show large net displacements but negative AC values.

153   In contrast, Type III trajectories (Fig. 2b, c, Supplementary Video 1) show small net

154   displacements with negative AC values, consistent with a confined motion of speckles.

155   In control cells, essentially all speckles showed locally confined, Type III trajectories. No

156   speckles (0/75) traveled further than 1.25 μm, and AC values were all below 0, with a total AC

157   range of ~ -2.0-0.0. In contrast, in DRB-treated cells, speckle mobility and AC values increased

158   significantly; 63% of speckle trajectories (Type I+Type II, 50/80) exhibited net distance

159   displacements, Δd, greater than 1.25 μm, with 14 out of 50 of these trajectories showing AC

160   values greater than 0 (Type I, Fig. 2b). Several of these speckles moved as far as 3 - 4 µm, nearly

161   three times as far as the largest displacement seen in control cells.

162   Plotting the distance moved as a function of time revealed that the subtrajectories

163   containing periods of long-range movement were predominately unidirectional with larger steps

164   than stationary movements shown before or after the long-range movement. (Fig. 2d). The

165   imprecision of the spatial alignment of nuclei between time points, due to changes in nuclear

166   shape, prevents us from determining to what degree small reverse speckle movements represent

167   true reverse speckle movements versus alignment errors. Projecting over time the 2D spatial

168   projections from multiple time points revealed the linear path of these subtrajectories containing

169   long-range directional movements (Supplementary Fig. 2).

170   **Repeated long-range, directional speckle movements all terminate with speckle fusion**

171   Strikingly, all the examples of long-range speckle movements shown in Fig. 2 and

172   Supplementary Fig. 2 terminate with a fusion between the smaller, mobile speckle and a larger,

173   relatively immobile speckle. These are not exceptional examples but rather the general rule

174   observed for nearly all long-range movements contained within a single observation period.

175   Fig. 3 shows all long-range speckle movements in two representative nuclei as examples.

176   Ten long-range speckle movements in nucleus 1 (Fig. 3a, Supplementary Video 2) end with

177   fusion to 7 larger speckles; in three cases, two different small speckles move long-distance, and

178   merge with the same larger speckle. Nine long-range speckle movements in nucleus 2 (Fig. 3B,

179   Supplementary Video 3) end with fusion to 5 larger speckles; three smaller speckles merge with

180   the same larger speckle in one case and two smaller speckles merge with the same larger speckle

181   in two other cases. Thus 19/19 long-range speckle trajectories terminate with fusion to a larger,

182   mostly immobile nuclear speckle.

183   Again, projecting over time the 3D spatial projections from multiple time points revealed

184   a largely curvilinear path for these long-range speckle trajectories, within the resolution of the

185   nuclear alignment between time points (Fig. 3a,b, top right panels).

186   Even more strikingly, in many cases we saw repeated long-range speckle movements in

187   which different nuclear speckles followed a very similar path to merge with the same single,

188   larger speckle. In the two nuclei shown in Fig. 3, 6/12 larger speckles are the fusion targets for

189   two or three mobile, smaller speckles. In each of these 6 examples, the second or even third

190   smaller nuclear speckle moves along essentially the same linear path, within the approximate

191   resolution of our nuclear alignment, to fuse with the larger speckle. Typically, after one speckle

192   began to move on a long-range trajectory, a new speckle would nucleate and enlarge, either at

193   the site of the first speckle prior to its movement (Fig. 4a,b, Supplementary Video 4) or along the

194   trajectory followed by the first speckle (Fig. 4c,d, Supplementary Video 4, Supplementary Fig.

195   3). The second speckle would later begin to move along a similar trajectory to the first and then

196   merge with the same speckle with which the first speckle moved.

197   We observed a number of cases in which three or even four speckles would appear in the

198   same or similar location, observing long-range movements of 2, 3, or even 4 of these speckles

199   along a similar trajectory before these speckles terminated their motion by fusion with the same

200   larger speckle (Fig. 4e, Supplementary Video 4). Furthermore, we observed examples in which

201   one speckle would merge with another, and then this merged speckle would move to fuse with a

202   third speckle (Fig. 3a, VII, Fig. 3b, V, Fig. 4d, 1:14:00-1:46:00).

203   These observations of long-range movements occurring through largely unidirectional

204   steps along curvilinear trajectories argue strongly for directional speckle movements along or

205   within a nuclear path or channel. This is strongly supported further by these observations of

206 repeated speckle movements along the same path or channel. Finally, as a further suggestion for

207 a mechanism leading to directed movements along a possible path, we observed that speckles

208 undergoing long-range movements would sometimes elongate in the direction of motion (Fig. 4b,

209 00:47:00, 1:09:00, Fig. 4e, 1:06:30) or the recipient speckle would form a long protrusion along

210 the path of the original smaller speckle trajectory (Fig. 3a, I, 00:53:00, III, 1:02:00, Fig. 3b, III,

211 1:06:00, 1:30:00, Fig. 4d, 2:22:00, Fig. 4e, 1:18:30).

212

213 **Viscoelastic behaviors of speckles and estimation of speckle viscosity**

214 During long-ranged speckle movements, we observed distinctive viscoelastic behaviors

215 such as "inchworm" or reptation motion, suggesting speckles as liquid-like bodies. For example,

216 a speckle would elongate in the direction of another speckle and then retract at the elongated end

217 nearest the target speckle to from a rounded speckle now closer to the target speckle; this was

218 then followed by a second round of elongation towards the target speckle followed by fusion and

219 then rounding into a single, larger speckle (Fig. 5a). In other cases, one speckle would

220 significantly elongate towards another target speckle until a long, linear speckle was formed that

221 would fuse with the target speckle; this would be followed by retraction of the elongated speckle

222 into the target speckle to form a single, rounded and larger speckle (Fig. 5b-d).

223 Furthermore, examination of speckle fusion events (Fig. 5e, f) supports the concept of

224 nuclear speckles as liquid-like nuclear bodies which have a similar viscosity as measured

225 previously for other liquid-like RNP bodies such as nucleoli and P granules[10, 11, 30]. We estimated

226 the viscosity of speckles by analyzing the time required after speckle fusion for a relaxation to a

227 circular shape in cells treated with DRB. As expected, relaxation times (τ) were linearly

228 proportional to the characteristic length scale (L) with a slope, which should approximate the

11

229   inverse capillary velocity, of 101 s/μm (Fig. 5h). This value is similar to previously measured

230   inverse capillary velocities of 2 s/μm for germline P granules of C. elegans[10], 46.1 s/μm for

231   nucleoli of *Xenopus* oocytes[11], and 125 s/μm for large RNP assemblies (grPB) in C. elegans

232   oocytes[30]. Assuming a speckle RNP granule size of ~20 nm, we obtained an estimated viscosity

233   (η) of speckles of $\sim 1 \cdot 10^3$ Pa·s, close to the measured viscosities of nucleoli ($\sim 2 \cdot 10^3$ Pa·s) and

234   grPB ($5 \cdot 10^3$ Pa·s).

235

236   **Long-range speckle motion does not require polymerized actin**

237   Previous examples of long-range chromosomal movements within interphase nuclei

238   suggested a direct or indirect role of actin, and in certain cases nuclear myosin 1C, in these

239   movements[31, 32]. To determine whether actin was involved in the long range motion of speckles,

240   we inhibited actin polymerization using latrunculin A (latA), and then measured the frequency

241   and length distributions of of long-range speckle movements.

242   LatA addition resulted in a decrease of long-range movements (Fig. 6a, Table 1). After

243   latA addition, long-range speckle movements greater than 1 μm were observed an average of 2.7

244   times per nucleus. This compared to an average of 9.8 long-range speckle movements per

245   nucleus in control cells. Although the frequency of long-range nuclear speckle movements was

246   significantly reduced, the distance distribution of these long-range speckle movements did not

247   significantly change with latA addition relative to those observed in control cells (Fig. 6a).

248   Similar types of long-distance speckle trajectories, also ending in fusion with a target speckle,

249   were observed after latA treatment (Fig. 6b, c, Supplementary Video 5).

250   To further test the possible involvement of actin in speckle motion, we transiently

251   transfected cells with plasmid constructs of actin fused to mRFP and a nuclear localization signal

252   (NLS) to concentrate this actin fusion protein in the nucleus[33, 34]. Different constructs were used

253   for expression of the wild type beta-actin sequence, a nonpolymerizable actin mutant[34] (G13R),

254   or an actin mutant that favors polymerized actin F-actin[33] (S14C).

255   Long-range nuclear speckle movements were observed in cells transfected (T) with all

256   three mRFP-NLS-actin mutants or mRFP-NLS- wild-type actin as well as nontransfected control

257   cells (U) (Table 1). The average number of long-range movements nuclear speckle movements

258   ranged from ~12-14 per nucleus. Mean distances of these speckle movements were also similar

259   (1.28-1.48 µm). The velocities of speckle movement during the periods of long-range movement

260   were also similar (~0.5-1.5 µm/min, data not shown).

261   Thus, we conclude that the observed long-range, directional movements of nuclear

262   speckles after DRB treatment are not actin-dependent.

263

264   **Nuclear speckles move in DAPI-depleted regions that are enriched with SON-granules**

265   To explore a possible structural basis for the repeated directed movement of small

266   nuclear speckles along the same apparent path towards a larger nuclear speckle, we used super-

267   resolution light microscopy. 3D structured illumination microscopy (SIM) and stimulated

268   emission depletion (STED) microscopy on fixed cells was complemented with correlative live-

269   cell in which we used conventional wide-field microscopy on live cells followed by fixation and

270   then SIM and STED imaging on the same cells.

271   Inspection of nuclear speckle movement in live-cell movies suggested the formation of

272   transient, faint connections of GFP-SON between nearby speckles (Supplementary Videos 6, 7).

273   Using STED microscopy, we could visualize individual, distinct SON-GFP granules that are in

274   the size range of STED resolution of ~60 nm and are distributed nonrandomly in the

13

275   nucleoplasm outside of nuclear speckles (Fig. 7). We used a combination of 3D SIM and STED

276   to visualize the relative distribution of chromatin and SON. 3D SIM of DAPI-stained, fixed

277   nuclei was followed by STED imaging of the same cells on a different STED microscope. These

278   DAPI SIM and anti-GFP-SON STED images were then aligned using a cross-correlation

279   procedure.

280   In these combined DAPI-SON images, we observed enrichment of SON granules in

281   DAPI-depleted spaces connecting nearby nuclear speckles, with most speckles appearing to be

282   connected by high local concentrations of these SON granules (Fig. 7a). These connections

283   persisted even after DRB treatment, even becoming clearer due to the reduced number of

284   granules overall in the nucleoplasm (Fig. 7a, right). The spatial distribution of these granules

285   suggests they are related to the faint, transient GFP-SON connections between nuclear speckles

286   visualized in our live-cell imaging.

287   We next used correlative live-cell and super-resolution imaging to determine the

288   relationship between the path followed by repeated nuclear speckle trajectories and these DAPI-

289   depleted, SON-granule-enriched spaces connecting neighboring nuclear speckles. After DRB

290   treatment, we followed live-cell imaging with immediate fixation of cells using

291   paraformaldehyde and staining. Inspection of the live-cell movies identified cells containing

292   examples of repeated speckle movements along a similar path terminated by fusion with the

293   same larger nuclear speckle. These cells were then identified and imaged by 3D SIM and STED.

294   These correlative images revealed that the path or channel along which nuclear speckles

295   had repeatedly moved was relatively DAPI-depleted but surrounded by DAPI stained chromatin

296   (Fig. 7b). Moreover, a relatively high concentration of SON granules was present within these

297   paths or channels relative to surrounding nuclear regions. Similar correlative results were

14

298   observed in cells treated with latA prior to addition of DRB (Fig. 7c).

299   Our observations of nuclear speckles moving within DAPI-depleted regions suggest that

300   chromatin may act as a barrier to speckle motion. We next used live-cell imaging to examine the

301   temporal correlation between changes in the DNA distribution surrounding nuclear speckles and

302   speckle movement and fusion events (Fig. 8). We used the cell-permeable, far-red SiR-Hoechst

303   dye that binds DNA in the minor grove like DAPI. Chromatin shows condensation with time

304   after DRB treatment, increasing the size of DNA-depleted intranuclear spaces (Fig. 8a). Fusion

305   between nearby large speckles indeed is temporally correlated with the disappearance of the

306   DNA staining observed in preceding time points within the space separating these same speckles

307   (Fig. 8b-e, Supplementary Videos 8, 9).

308

309   **Similar long-range and repeated speckle movements after heat-shock**

310   To place our observations within a more physiological context, we examined speckle

311   dynamics during heat shock. After heat shock, while most genes are transcriptionally down-

312   regulated 5-fold or more (Mahat, 2016), heat-shock genes are induced up to 200-fold (Lis, 1981,

313   Mahat, 2016). Previously, we demonstrated that heat-shock transcriptional induction of Hsp70

314   plasmid transgene arrays was greatly enhanced after nuclear speckle contact (Khanna et al. 2014).

315   Similar to DRB treatment, after heat shock we observed multiple examples of long-range

316   motions of smaller nuclear speckles terminating with fusion with larger nuclear speckles.

317   Supplementary Fig. 4 shows a striking example of repeated nucleation of new speckles adjacent

318   to the Hsp70 transgene array followed by long-range motion of these speckles towards a larger,

319   distant nuclear speckle. Later, speckles nucleate along this speckle trajectory and then merge to

320   form a continuous, ~ 4 μm long connection between the transgene array and distant speckle.

321   Supplementary Fig. 5 shows a long-range speckle motion terminating after association with the

322   Hsp70 BAC transgene array which then shows an abrupt increase in its transcription.

323

Discussion

324

325   Here we showed an increased mobility of nuclear speckles after transcriptional inhibition

326   by DRB, including prominent long-range movements of smaller speckles over distances of 1-4

327   um with velocities 0.2-1.5um/min that typically terminated through fusion with a larger speckle.

328   These long-range movements appeared directional, following roughly linear trajectories pointing

329   to and ending with merging in pre-existing stationary speckles. Speckles frequently elongated in

330   the direction of movement during these movements, suggesting the possibility of an active

331   transport mechanism. Directionality was also inferred based on our observations of repeated

332   cycles of nucleation of new speckles and their movement along similar trajectories followed by

333   previous moving speckles. These long-range, speckle movements occurred independent of

334   polymerized nuclear actin as their length distribution was unchanged after lantrunculin A

335   treatment. Correlation of live-cell imaging with super-resolution microscopy on fixed samples

336   revealed that speckles moved within channels relatively depleted of DNA but enriched in SON-

337   protein containing granules.

338   As observed previously, upon transcriptional inhibition speckles became rounder and

339   larger. This increase in speckle size was imagined to occur as a result of RNA processing

340   components being released from previous sites of transcription, diffusing into speckles, and then

341   accumulating within the speckle through binding to other components[23, 35]. Dephosphorylation of

342   SR proteins was proposed to lead to their accumulation in speckles, while phosphorylation of SR

343   proteins was proposed to lead to their release from speckles, diffusion into the nucleoplasm, and

344   binding to local transcription sites[36, 37]. Consistent with this model, modeling the mobility of

345   speckle proteins as measured by FRAP (Fluorescence Recovery After Photobleaching) led to the

346   conclusion that differential nuclear distribution of splicing factors was controlled by changes in

17

347   their binding to either nucleoplasmic or speckle sites[38, 39, 40].

348   Not explained by these studies was how the number of speckles decreases with

349   transcriptional inhibition. Also these previous studies proposed that the increased size of

350   speckles after transcriptional inhibition is entirely due to diffusion of speckle components from

351   the nucleoplasm followed by binding to sites within speckles.

352   Our results instead suggest that a significant cause of both the increase in individual

353   speckle size and brightness and the reduction in speckle number is through the directed, long-

354   range movements of speckles towards other speckles followed by their fusion. Future work will

355   be needed to determine the relative contributions of diffusion and binding of speckle components

356   versus speckle fusion events to the observed increase in speckle size observed after

357   transcriptional inhibition. Future work also will be needed to determine whether posttranslational

358   modifications of speckle proteins are also connected to directional motion and/or fusion of

359   speckles.

360   During the dynamic movement of speckles, we confirmed liquid-state properties of

361   nuclear speckles. Speckles exhibited nucleation, deformation in the direction of translocation,

362   and fusion. Strikingly, we found that motion of speckles after transcriptional inhibition always

363   ended with fusion with another speckle. After fusion, speckles regained their circular shape but

364   were bigger and showed an increased intensity, suggesting mixing of constituent molecules as

365   seen in liquid-phase cellular bodies[41]. Analysis of the time interval between speckle fusion and

366   rounding of the merged speckles allowed us to estimate the viscosity of nuclear speckles, which

367   we found was similar to previously measured viscosities for *Xenopus* oocyte nucleoli and grPBs

368   of *C. elegans* oocytes. Not considered in our analysis was the possibility that adjacent chromatin

369   interacting with nuclear speckles might slow the rounding of the nuclear speckle after fusion

18

370   events. Therefore, our estimates of nuclear speckle viscosity might be best considered an upper

371   bound on the actual speckle viscosity, where the actual viscosity nuclear speckles might be

372   somewhat lower depending on how significant these chromatin interactions might be on the

373   actual relaxation time of the speckles after fusion. Overall, though, these measurements indicate

374   that nuclear speckles possess viscoelastic properties and behaviors similar to those observed in

375   other RNP bodies.

376   Significantly, although the frequency of long-range speckle movements decreased after

377   perturbation of actin polymerization, the length distributions of these speckle movements did not

378   change. Therefore, the long-range, directed movement of speckles after transcriptional inhibition

379   is not dependent on polymerized actin. This rules out a more conventional actin-myosin based

380   mechanism for speckle motility, despite reports of nuclear myosin I isoforms in nuclear speckles

381   and enrichment of these isoforms in speckles after transcription inhibition[42].

382   Fusion between nearby speckles to form larger speckles could be explained as driven by

383   collisions between speckles mediated through random Brownian motion. However, our

384   observation of directed motion of speckles over distances up to several microns in length, in

385   many cases followed by a new speckle moving along a similar path, requires a different

386   explanation than random diffusion.

387   One possible clue pointing to a potential mechanism underlying speckle long-range

388   motion might be our observation of SON-containing granules concentrated in DAPI-poor

389   channels connecting nearby speckles. Correlative live-cell / fixed-cell imaging revealed that

390   these channels roughly co-localized to the path of actual speckle movements observed in live-

391   cells shortly before fixation. We can envision more than one scenario that might give rise to

392   these localized SON-granule accumulations on the path of speckle movements.

393   A flow of SON-granules between neighboring speckles, through some unknown

394   mechanism(s), might establish this concentration of granules. Numerical modeling of a simple

395   binary fluid mixture predicts a net flux of individual components through diffusion from small to

396   larger droplets due to the greater stability of the larger droplets because of their lower interface

397   free energy. Moreover, this net flux generates a composition correlation between two

398   neighboring droplets of different sizes, leading to an intradroplet gradient of interfacial tension

399   and producing a hydrodynamic flow of small droplets towards larger droplets followed by

400   droplet fusion[43]. Interestingly, this modeled behavior of droplet movements in simple binary

401   fluid mixtures mirrors our observation of small speckles moving towards larger speckles.

402   Additionally, movement of one speckle along a trajectory might leave SON-granules along its

403   path- analogous to tiny droplets of water left behind by movement of a large water droplet along

404   a surface. These pre-positioned SON-granules speckles might work as "steps" biasing

405   movements of other speckles at later times. Finally, we cannot rule out an active, but unknown

406   transport mechanism driving speckle movements. Additional experiments including future live-

407   cell imaging at higher temporal and spatial resolution will be needed to explore these ideas.

408   Our correlative imaging using SIM, STED and live-cell imaging also allowed us to

409   determine the relative spatial arrangement between chromatins and speckles. The movement of

410   speckles occurred within the interchromatin space, with chromatin seen surrounding the speckles

411   and the apparent channels through which the speckles moved, suggesting that chromatin may act

412   as a spatial barrier to speckle movement and confine these movements to linear trajectories.

413   Indeed, under normal growth conditions, we observed speckle mobility consistent with confined

414   motion. The observed directional motion after transcriptional inhibition is consistent with a

415   release of constraints to speckle motion as a result of the chromatin condensation observed in

416   live-cell movies after transcriptional inhibition. Thus, we suspect that chromatin in nuclei plays a

417   similar constraining role in restricting translocation and fusion of nuclear speckles as actin

418   networks have been shown to play in constraining movement and coalescence of

419   ribonucleoprotein droplets and nucleoli in oocytes[11, 44].

420   In conclusion, in this study, the most striking aspects of the long-range speckle

421   movement we observed were the repeated cycles of speckle nucleation, translocation of the

422   newly nucleated speckles along a similar trajectory as that followed by preceding speckles, and

423   then fusion with the same target speckle. Together these observations point to a previously

424   unsuspected cellular trafficking system for movement and nuclear positioning of nuclear

425   speckles. We anticipate these non-random speckle movements may provide a rapid and effective

426   transport of RNA processing and/or transcription factors to specific nuclear sites. Moreover,

427   recent identification of genomic regions that associate at near 100% frequencies with nuclear

428   speckles[45] suggest that the nuclear positioning of speckles may also drive nuclear genome

429   organization. The phenomenology of nuclear speckle movements described here should allow

430   future development of assays that can be used to identify the molecular components of

431   responsible for this nuclear speckle cellular trafficking system.

432

433

434

435

Materials and methods

Cell culture and establishment of cell line

CHOK cells were grown in F12 media (Cell media facility, University of Illinois at Urbana-Champaign) supplemented with 10% Fetal Bovine Serum (Sigma-Aldrich, F2442) at 37°C in 5% CO_2. To generate a stable cell line expressing EGFP fused to the SON protein, we used a BAC EGFP-SON transgene (EGFP-SON-Zeo BAC) in which a starting BAC containing a human SON genomic insert (RP11-165J2, Invitrogen) was retrofitted using BAC recombineering to add a Zeocin selectable marker and the EGFP sequence in frame with the SON NH2 terminus (Khanna, Hu, and Belmont 2014). We purified the EGFP-SON-Zeo BAC using the Large-Construct Kit (Qiagen). 5ug of the purified construct was linearized with BsiWI(NEB), followed by incubation at 65   for 20 mins to inactivate BsiWI. CHOK cells were transfected with the linearized EGFP-SON-Zeo BAC using Lipofectamine 2000 (Invitrogen) one day after passaging while at ~60% confluency following the manufacturer's suggested protocol. After 36 hours, transfected cells were trypsinized (Trypsin-EDTA 0.25%, Gibco) and transferred to a larger flask to which selection media (200 μg/ml Zeocin, ThermoFisher) was added. After 10 days of selection, cells were subcloned by serial dilution into 96-well plates. Individual subclones were screened by microscopy using a Deltavision wide-field microscope (GE Healthcare) to select clones which showed uniform and stable EGFP-SON expression.

Drug treatments

To add drugs without adding new serum, we removed half the media from the cell culture dishes, added chemicals to a 2x concentration using this media, and then returned this media back to the same dishes. The final DRB working concentration was 50μg/ml (Sigma, 50mg/ml stock solution in DMSO). Other drugs were used at the following working (and stock) concentrations: 50ug/ml α-Amanintin (A2263, Sigma, 1mg/ml in DI water), 0.1ug/ml triptolide (T3652, Sigma, 1mg/ml in DMSO), 200uM Cd solution (20920, Sigma, 100mM in DI water). For live cell imaging, chemicals were prepared in the same way, and returned to the live cell dish on the microscope.

For latrunculin A (latA) treatment (L5163, Sigma), cells were seeded on poly-L-lysine coated coverslips or glass-bottom dishes (Mattek). Coverslips or glass-bottom dishes (Mattek) were covered with 0.01% Poly-L-lysine solution (P4707, Sigma) for 10 mins, rinsed with sterilized DI

467 water, and dried in the tissue culture hood. Cells were grown two days on these coated surfaces,

468 treated with 1uM latA for 30 mins, and then with DRB as described above.

469

Sample preparation for fixed cell imaging

471 For quantitative analysis of speckle morphology, cells were seeded on coverslips (Fisher)

472 and fixed 48 hrs later at ~90-100% confluency using freshly prepared 3.6% paraformaldehyde

473 (PFA, Sigma, P6148-500G) in PBS for 20 mins at room temperature. After three times of

474 washing for 5minutes each in phosphate-buffered saline (PBS), the fixed cells were then

475 mounted in a Mowiol-DABCO anti-fade medium[46].

476 For STED and SIM imaging, immunofluorescence and DAPI staining were done after

477 fixation and 3x 5min washes in PBS. For immunofluorescence staining, cells were incubated in

478 blocking buffer (0.5 % Triton X-100 (Thermo Fisher) and 0.5 % normal goat serum (Sigma-

479 Aldrich) in PBS for 30 mins. Cells were then incubated with monoclonal anti-SON primary

480 antibodies (1:300 in PBS; Sigma-Aldrich) overnight at 4°C. After 3x 5min washes in PBS, cells

481 were incubated with Atto647N-conjugated goat anti-rabbit IgG (1:300 in PBS; ATTO-TEC) for

482 2 hrs at room temperature, and then washed 3x for 5mins each in PBS. The cells were postfixed

483 with 3.6% PFA for 15 mins, and washed 3x 5min in PBS. Cells were counterstained with 1ug/ml

484 DAPI (Sigma-Aldrich) in PBST (0.1% Triton X-100 in PBS) for 0.5-1 hr at room temperature

485 (Smeets et al. 2014), and then washed 5x for 5 mins each in PBS. We equilibrated the cell

486 samples with Vectashield antifade mounting medium (H-1000, Vector Laboratories) for 10 mins,

487 aspirated the media, and added fresh mounting medium. This was repeated 3-5times to

488 completely infiltrate the cells with the mounting medium to avoid refractive index changes over

489 the cells. Coverslips were mounted on slides and sealed with nail polish.

490

Microscopy of fixed samples and analysis of cell morphology

492 We used a Deltavision wide-field microscope (GE Healthcare), equipped with a Xenon

493 lamp, 60X, 1.4 NA oil immersion objective (Olympus) and CoolSNAP HQ CCD camera (Roper

494 Scientific). 1024x1024 pixel 2D images were acquired as 3D z-stacks and processed using the

495 "Enhanced" version of the iterative, nonlinear deconvolution algorithm provided by the Softworx

496 software[47] (GE Healthcare). 3D deconvolved image stacks were projected into 2D using a

497 maximum intensity algorithm.

498   Analysis of speckle morphology used custom Matlab codes for image segmentation in

499   several sequential steps. Multiple intensity thresholds and image segmentation steps allowed us

500   to segment speckles of varying sizes and intensity levels. We first automatically choose an initial

501   intensity threshold using Matlab's *graythresh* function (*graythresh**1.5~1.8) based on Otsu's

502   method (Otsu, 1979). This allowed us to produce a binary image from which we measured area,

503   perimeter, and form factor (FF= $4*\pi*$Area/(Perimeter)^2) of the larger, brighter speckles. To

504   calculate intensities of these speckles, we used the segmented areas as a mask which was applied

505   to a new 2D projected image generated by an intensity projection from the original 3D raw

506   image stacks. The normalized speckle intensity was calculated by summing the intensities of all

507   pixels within a speckle, subtracting the background intensity over an equivalent area and then

508   normalizing by the speckle area ({Sum of pixel values in speckle- (mean value of nuclear

509   background*size of the speckle)}/Size of speckle). Once these large speckles were segmented

510   and analyzed, we removed them from the deconvolved projected image by replacing their pixel

511   intensities equal to the cellular background level. We then repeated the image thresholding,

512   setting a new intensity threshold using the *graythresh* function (*graythresh*0.8~1.8*), and

513   repeating the same process as described above to measure a new set of speckles and then remove

514   them from the image. If necessary, this process was repeated one more time to select the

515   remaining small speckles. To prevent the situation in which part of a speckle that was not

516   segmented in a previous cycle was counted as a new speckle, at each step we recorded the

517   coordinates of segmented speckle centers and discarded any new speckles in a subsequent cycle

518   that were within 0.3 μm of a previous speckle center. Through 3 such segmentation cycles, we

519   were able to identify and measure the morphology of most speckles present in the nucleus.

520   However, very small speckles less than 0.4 μm diameter were not considered in our

521   measurements of changes in speckle morphology before and after transcriptional inhibition.

522

523   **Live cell imaging and tracking.**

524   For live cell imaging, we used a V3 OMX (GE healthcare) microscope, equipped with a

525   100X, 1.4 NA oil immersion objective (Olympus), two Evolve EMCCDs (Photometrics), a live-

526   cell incubator chamber for CO_2 perfusion, and two temperature controllers for the incubator and

527   the objective lens heaters. Temperatures of the live cell chamber and lens were maintained at

528   37   . Cells were seeded in glass-bottom dishes (Mattek) to reach ~90-100% confluency 48 hrs

24

529   later. 3D stacks (z-spacing 300nm) were acquired in the conventional wide-field imaging mode

530   at given time intervals, followed for each time point by 3D deconvolution and 2D maximum

531   intensity projection using the Softworx software. Image J was used first to smooth these

532   projections with a Gaussian filter (σ=2). Then a rigid body registration (ImageJ plugin

533   'StackReg') was applied to correct for any x-y nuclear rotation and/or translational displacement

534   between sequential time points. A region including a full speckle motion was cropped from the

535   image manually using ImageJ, and the single speckle was tracked by custom Matlab code. The

536   cropped image was transformed into a binary image by the intensity threshold selected by

537   Matlab's *graythresh* function. The center of mass of the speckle was then determined over time

538   by Matlab's *regionprops* function and used for speckle tracking.

539

540   **Viscosity analysis**

541   To estimate nuclear speckle viscosity, we acquired live cell movies using a 5 sec time

542   interval over 90 mins. We identified nuclear speckles undergoing fusion and measured their long

543   axes (l_{long}) and short axes (l_{short}) to calculate as a function of time their aspect ratio (AR), defined

544   as AR=l_{long}/l_{short}. A relaxation time (τ) for the speckle fusion was estimated by fitting the

545   measured AR to the exponential decay curve defined by AR= P+(AR$_0$-P)$\cdot$e$^{-t/\tau}$, where P is the

546   plateau of the exponential curve and AR$_0$ is the AR at time=0.

547   The length scale was calculated as L =$[(l_{long} - l_{short})\cdot l_{short}]^{0.5}$ at time=0, and plotted against τ.

548   From a linear fit of τ vs. L by least-squares estimation, we obtained the slope that corresponds to

549   the inverse capillary velocity (η/γ), where η is the viscosity and γ the surface tension[48]. We could

550   estimate $\gamma \approx k_bT/d^2$ [49], where k_b is the Boltzmann constant, T is the temperature, and d is

551   molecular length scale (~10nm used for RNAPs in previous studies[11, 30]). We used ~20 nm for

552   the characteristic RNP granules contained within IGCs[15, 16]. From the estimated γ and the inverse

553   capillary velocity (η/γ), we estimated the viscosity of nuclear speckles.

554

555   **Correlative live cell imaging and super-resolution imaging**

556   To combine live-cell imaging with STED and SIM, cells were seeded in glass-bottom

557   dishes engraved with 50 μm grid pattern, letters and numbers (81148, Ibidi), reaching ~60-70%

558   confluency 2 days later. Prior to live cell imaging, we recorded locations of target cells using the

559   alphanumeric characters to find the same target cells later when we used different microscopes.

560   After live-cell imaging, cells were immediately fixed by adding 2x PFA solution in PBS to the

561   cell media. The final PFA concentration was 4%. Immunofluorescence and DAPI staining

562   followed by mounting in Vectashield anti-fade medium were done as described above.

563   For STED images, we used a custom made STED microscope[50], and acquired 3D z-

564   stacks through the entire SON immunofluorescent stained nucleus using 300 nm z-spacing.

565   3D-SIM images were acquired on the V3 OMX microscope (see above) using 0.125 um

566   z-spacing and sequential excitation at 488 and 405 nm on each image plane. Each z-stack image

567   contained 15 images at 5 different phases per angle and 3 different angles per slice. We collected

568   a full 3D-SIM image of GFP-SON and DAPI-staining. 3D-SIM image stacks were reconstructed

569   with Softworx. The chromatic aberration offset between the GFP and DAPI wavelengths was

570   measured with the alignment slide provided by GE Healthcare and used to correct the 3D-SIM

571   images using the OMX Image registration function in Softworx.

572   To align the STED SON and SIM DAPI images, we selected a single STED optical z-

573   section showing speckles of interest and then matched it to the most similar optical z-section

574   from the complete stack of the 3D SIM GFP-SON image. Since 2D STED imaging was done

575   using a 300 nm z-interval (z resolution ≈ 600 nm), we used the 2D projection of 3 adjacent SIM

576   z-sections, consisting of the most similar SIM optical section plus the SIM optical sections

577   immediately above and below this optical section. Because 'StackReg' registration tool in

578   ImageJ required a combined stack of images, we matched x-y sizes of SIM image (1024x1024

579   pixels, pixel size= 40nm after reconstruction) and STED image (varying, pixel size=20~40nm)

580   by adding pixels of background intensity or by taking a certain size of sub-region from a large

581   image. We then generated a RGB SIM image from DAPI (blue) and SON (green) after saturating

582   SON intensity to be used as a reference for alignment with STED image. We finally combined

583   RGB SIM image and STED SON as z-stacks, and ran 'StegReg' with rigid body mode. In this

584   way, STED SON image could be easily aligned on the strong SON signal of the SIM image,

585   where SIM DAPI image and SIM SON image were grouped during alignment process. From the

586   aligned z-stacks, we took SIM DAPI image and STED SON image.

587

588   **Live cell imaging and analysis of chromatin compaction after DRB treatment**

589   To visualize chromatin structure in live cells, we incubated cells growing in glass-bottom

590   dishes with 100 nM SiR-Hoechst (Spirochrome, SC007) for 1 hr before imaging. We started 3D

26

591 live-cell imaging immediately after adding DRB, acquiring simultaneously both GFP-SON

592 (excitation at 488nm) and SiR-Hoescht (excitation at 642nm) images for 2 hrs using a 1 min time

593 interval. Deconvolution and maximum intensity 2D projection at each time point were performed

594 by Softworx as described previously. We converted these time-lapse 2D projected images into

595 binary images by segmentation using ImageJ plugin 'Threshold' based on the Otsu thresholding

596 method[51]. From these segmented binary chromatin images, we computed the chromatin area as a

597 function of time using the Matlab's *'regionprops'* function.

598
599 **Acknowledgements**

603
604 **Author contributions**

605 J.K. and A.S.B. conceived and designed experiments. J.K. conducted experiments, analyzed data.

606 K.Y.H. acquired STED images, contributed on data analysis and experimental design. N.K.

607 contributed to generate cell lines. A.S.B. and T.H. supervised the project. J.K. and A.S.B. wrote

608 the paper with feedback from other authors.

609
610 **Competing interests**

611 All authors declare no competing financial interests.

612

References

1. Banks DS, Fradin C. Anomalous diffusion of proteins due to molecular crowding. *Biophysical Journal* **89**, 2960-2971 (2005).

2. Cremer T, Cremer C. Chromosome territories, nuclear architecture and gene regulation in mammalian cells. *Nature Reviews Genetics* **2**, 292-301 (2001).

3. Weidemann T, Wachsmuth M, Knoch TA, Müller G, Waldeck W, Langowski J. Counting nucleosomes in living cells with a combination of fluorescence correlation spectroscopy and confocal imaging. *Journal of Molecular Biology* **334**, 229-240 (2003).

4. Hyman AA, Weber CA, Juelicher F. Liquid-liquid phase separation in biology. *Annual Review of Cell and Developmental Biology* **30**, 39-58 (2014).

5. Zhu L, Brangwynne CP. Nuclear bodies: The emerging biophysics of nucleoplasmic phases. *Current Opinion in Cell Biology* **34**, 23-30 (2015).

6. Han TNW*, et al.* Cell-free formation of RNA granules: Bound RNAs identify features and components of cellular assemblies. *Cell* **149**, 768-779 (2012).

7. Kaiser TE, Intine RV, Dundr M. De novo formation of a subnuclear body. *Science* **322**, 1713-1717 (2008).

8. Kato M*, et al.* Cell-free formation of RNA granules: low complexity sequence domains form dynamic fibers within hydrogels. *Cell* **149**, 753-767 (2012).

9. Schwartz JC, Wang X, Podell ER, Cech TR. RNA seeds higher-order assembly of FUS protein. *Cell Reports* **5**, 918-925 (2013).

10. Brangwynne CP*, et al.* Germline P granules are liquid droplets that localize by controlled dissolution/condensation. *Science* **324**, 1729-1732 (2009).

11. Brangwynne CP, Mitchison TJ, Hyman AA. Active liquid-like behavior of nucleoli determines their size and shape in Xenopus laevis oocytes. *P Natl Acad Sci USA* **108**, 4334-4339 (2011).

12. Aizer A, Brody Y, Ler LW, Sonenberg N, Singer RH, Shav-Tal Y. The dynamics of mammalian P body transport, assembly, and disassembly in vivo. *Molecular Biology of the Cell* **19**, 4154-4166 (2008).

13. Buchan JR, Parker R. Eukaryotic stress granules: the ins and outs of translation. *Mol Cell* **36**, 932-941 (2009).

655 14. Dundr M*, et al.* In vivo kinetics of Cajal body components. *Journal of Cell Biology* **164**, 831-
656   842 (2004).
657

658 15. Spector DL. Macromolecular domains within the cell-nucleus. *Annual Review of Cell Biology*
659   **9**, 265-315 (1993).
660

661 16. Thiry M. The interchromatin granules. *Histology and Histopathology* **10**, 1035-1045 (1995).
662

663 17. Carter KC, Taneja KL, Lawrence JB. Discrete nuclear domains of poly(A) RNA and their
664   relationship to the functional-organization of the nucleus. *Journal of Cell Biology* **115**, 1191-
665   1202 (1991).
666

667 18. Mintz PJ, Patterson SD, Neuwald AF, Spahr CS, Spector DL. Purification and biochemical
668   characterization of interchromatin granule clusters. *EMBO Journal* **18**, 4308-4320 (1999).
669

670 19. Saitoh N, Spahr CS, Patterson SD, Bubulya P, Neuwald AF, Spector DL. Proteomic analysis of
671   interchromatin granule clusters. *Molecular biology of the cell* **15**, 3876-3890 (2004).
672

673 20. Lamond AI, Spector DL. Nuclear speckles: a model for nuclear organelles. *Nature Reviews*
674   *Molecular cell biology* **4**, 605-612 (2003).
675

676 21. O'Keefe RT, Mayeda A, Sadowski CL, Krainer AR, Spector DL. Disruption of pre-mRNA
677   splicing in vivo results in reorganization of splicing factors. *Journal of Cell Biology* **124**, 249-260
678   (1994).
679

680 22. Spector DL, Fu XD, Maniatis T. Associations between distinct pre-mRNA splicing components
681   and the cell nucleus. *The EMBO journal* **10**, 3467-3481 (1991).
682

683 23. Misteli T, Cáceres J, Spector D. The dynamics of a pre-mRNA splicing factor in living cells.
684   *Nature* **387**, 523-527 (1997).
685

686 24. Khanna N, Hu Y, Belmont AS. Hsp70 transgene directed motion to nuclear speckles
687   facilitates heat shock activation. *Current Biology* **24**, 1138-1144 (2014).
688

689 25. Sharma A, Takata H, Shibahara K-I, Bubulya A, Bubulya PA. Son Is Essential for Nuclear
690   Speckle Organization and Cell Cycle Progression. *Molecular Biology of the Cell* **21**, 650-663
691   (2010).
692

693 26. Boucher L, Ouzounis CA, Enright AJ, Blencowe BJ. A genome-wide survey of RS domain
694   proteins. *Rna-a Publication of the Rna Society* **7**, 1693-1701 (2001).
695

696 27. Bensaude O. Inhibiting eukaryotic transcription: Which compound to choose? How to
697   evaluate its activity? *Transcription* **2**, 103-108 (2011).
698

29

28. Yankulov K, Yamashita K, Roy R, Egly JM, Bentley DL. The transcriptional elongation inhibitor 5,6-dichloro-1-beta-D-ribofuranosylbenzimidazole inhibits transcription factor IIH-associated protein kinase. *The Journal of biological chemistry* **270**, 23922-23925 (1995).

29. Izeddin I*, et al.* Single-molecule tracking in live cells reveals distinct target-search strategies of transcription factors in the nucleus. *Elife* **3**, (2014).

30. Hubstenberger A, Noble SL, Cameron C, Evans TC. Translation repressors, an RNA helicase, and developmental cues control RNP phase transitions during early development. *Developmental Cell* **27**, 161-173 (2013).

31. Chuang CH, Carpenter AE, Fuchsova B, Johnson T, de Lanerolle P, Belmont AS. Long-range directional movement of an interphase chromosome site. *Current Biology* **16**, 825-831 (2006).

32. Dundr M*, et al.* Actin-dependent intranuclear repositioning of an active gene locus in vivo. *Journal of Cell Biology* **179**, 1095-1103 (2007).

33. Posern G, Miralles F, Guettler S, Treisman R. Mutant actins that stabilise F-actin use distinct mechanisms to activate the SRF coactivator MAL. *The EMBO Journal* **23**, 3973-3983 (2004).

34. Posern G, Sotiropoulos A, Treisman R. Mutant actins demonstrate a role for unpolymerized actin in control of transcription by serum response factor. *Molecular biology of the cell* **13**, 2001-2015 (2002).

35. Jimenez-Garcia LF, Spector DL. In vivo evidence that transcription and splicing are coordinated by a recruiting mechanism. *Cell* **73**, 47-59 (1993).

36. Colwill K*, et al.* The Clk/Sty protein kinase phosphorylates SR splicing factors and regulates their intranuclear distribution. *Embo Journal* **15**, 265-275 (1996).

37. Misteli T, Cáceres JF, Clement JQ, Krainer AR, Wilkinson MF, Spector DL. Serine phosphorylation of SR proteins is required for their recruitment to sites of transcription in vivo. *Journal of Cell Biology* **143**, 297-307 (1998).

38. Kruhlak MJ, Lever MA, Fischle W, Verdin E, Bazett-Jones DP, Hendzel MJ. Reduced mobility of the alternate splicing factor (ASF) through the nucleoplasm and steady state speckle compartments. *Journal of Cell Biology* **150**, 41-51 (2000).

39. Phair RD, Misteli T. High mobility of proteins in the mammalian cell nucleus. *Nature* **404**, 604-609 (2000).

40. Rino J, Carvalho T, Braga J, Desterro JMP, Lührmann R, Carmo-Fonseca M. A stochastic view of spliceosome assembly and recycling in the nucleus. *PLoS Computational Biology* **3**, 2019-2031 (2007).

743

744   41. Brangwynne CP. Phase transitions and size scaling of membrane-less organelles. *Journal of*
745   *Cell Biology* **203**, 875-881 (2013).

746

747   42. Ihnatovych I, Migocka-Patrzalek M, Dukh M, Hofmann WA. Identification and
748   characterization of a novel myosin Ic isoform that localizes to the nucleus. *Cytoskeleton* **69**,
749   555-565 (2012).

750

751   43. Shimizu R, Tanaka H. A novel coarsening mechanism of droplets in immiscible fluid mixtures.
752   *Nat Commun* **6**, 7407 (2015).

753

754   44. Feric M, Brangwynne CP. A nuclear F-actin scaffold stabilizes ribonucleoprotein droplets
755   against gravity in large cells. *Nature Cell Biology* **15**, 1253-1259 (2013).

756

757   45. Chen Y, *et al.* TSA-Seq mapping of nuclear genome organization. *bioRxiv*, doi:
758   10.1101/307892 (2018).

759

760   46. Ed Harlow DL. *Antibodies. A laboratory manual.* Cold Spring Harbor Laboratory (1988).

761

762   47. Agard DA, Hiraoka Y, Shaw P, Sedat JW. Fluorescence Microscopy in 3 Dimensions. *Methods*
763   *in Cell Biology* **30**, 353-377 (1989).

764

765   48. Eggers J. Nonlinear dynamics and breakup of free-surface flows. *Reviews of Modern Physics*
766   **69**, 865-929 (1997).

767

768   49. Aarts DGAL, Schmidt M, Lekkerkerker HNW. Direct visual observation of thermal capillary
769   waves. *Science* **304**, 847-850 (2004).

770

771   50. Han KY, Ha T. Dual-color three-dimensional STED microscopy with a single high-repetition-
772   rate laser. *Optics Letters* **40**, 2653-2656 (2015).

773

774   51. Otsu N. Threshold selection method from gray-level histograms. *IEEE Trans Syst Man Cybern*
775   **9**, 62-66 (1979).

776

777

778

779
780

	Number of cells	Average number of long-range movements per cell	Average distance(μm)
Control	16	9.8	1.53
LatA	18	2.7	1.50
WT actin(T)	17	13.4	1.48
WT actin (U)	17	12.8	1.48
G13R actin(T)	20	12.3	1.28
G13R actin(U)	15	12.2	1.28
S14C actin(T)	17	14	1.38
S14C actin(U)	22	13.5	1.34

781
782 **Table 1. Numbers of long-range speckle movements (>1 μm) per nucleus in cells treated with**
783 **latA or expressing an actin mutant after DRB addition.** "T" stands for transfected cells with
784 indicated actin construct, "U" stands for non-transfected control cells in same cell dish. LatA
785 was added 30 mins prior to DRB addition. DRB was added at time 0, and time-lapse
786 measurements were made from 30-90 mins after DRB treatment.
787

788
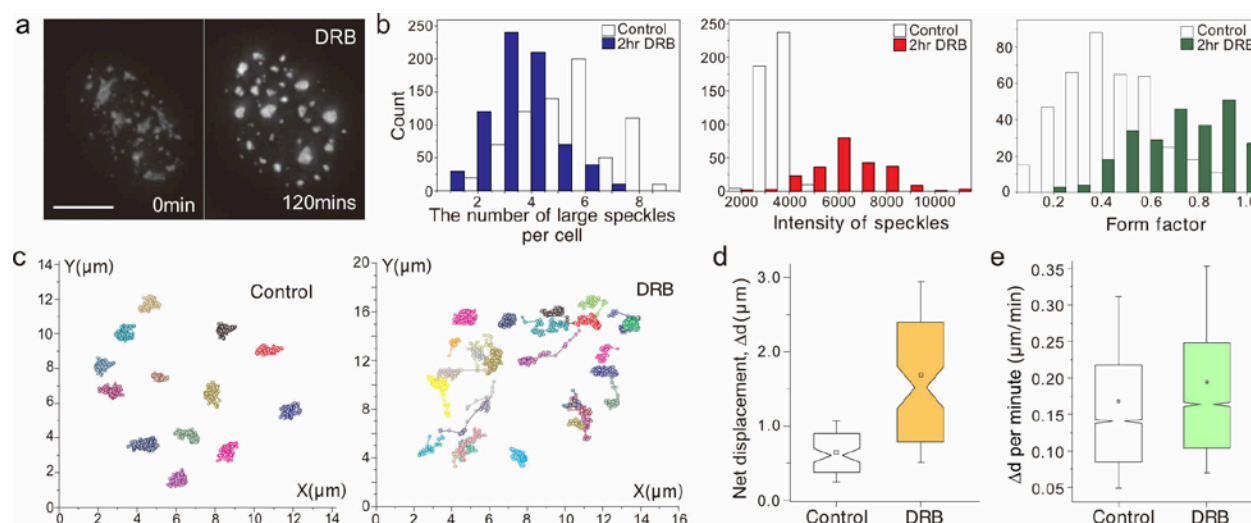
Figure 1. Inhibition of RNA polymerase II transcription by DRB changes speckle morphology and increases speckle mobility. a. Changes in speckle morphology, visualized using GFP-SON, before and after DRB addition. Scale bar: 5μm. **b.** Measurement of speckle number (>1 um in diameter) (left), intensity (middle), and shape (right) (Form Factor (FF)) before and after 2 hrs DRB treatment. Large speckles reduce in number (blue), become brighter (~2.5 fold, red), and rounder (1.5-fold increase in FF, green) after DRB addition. **c.** Speckle trajectories before and after DRB addition. Speckles, each assigned a different color, were tracked over a 1 hr period in control (left) and DRB-treated cell (right). **d.** Net displacement (Δd) of speckles measured in control (white) and DRB-treated cells (yellow). Speckle displacements increase after DRB addition (p-value = 1.007e-12; Paired student's t-test). Boxplot: Box- mean (square inside box), median (notch of box), 25 (bottom) and 75 (top) percentiles; ends of error bars- 10 (bottom) and 90 (top) percentiles. n=75 speckles from 10 control cells, n=80 speckles from 10 DRB treated cells. **e.** Displacement (Δd) per minute increases from before (white) to after DRB addition (green) (p-value=2.2e-16; paired Wilcoxon signed rank test) Boxplots as in (d). n=4487 steps from 49 speckles (control), n=4375 steps from 50 speckles (DRB).
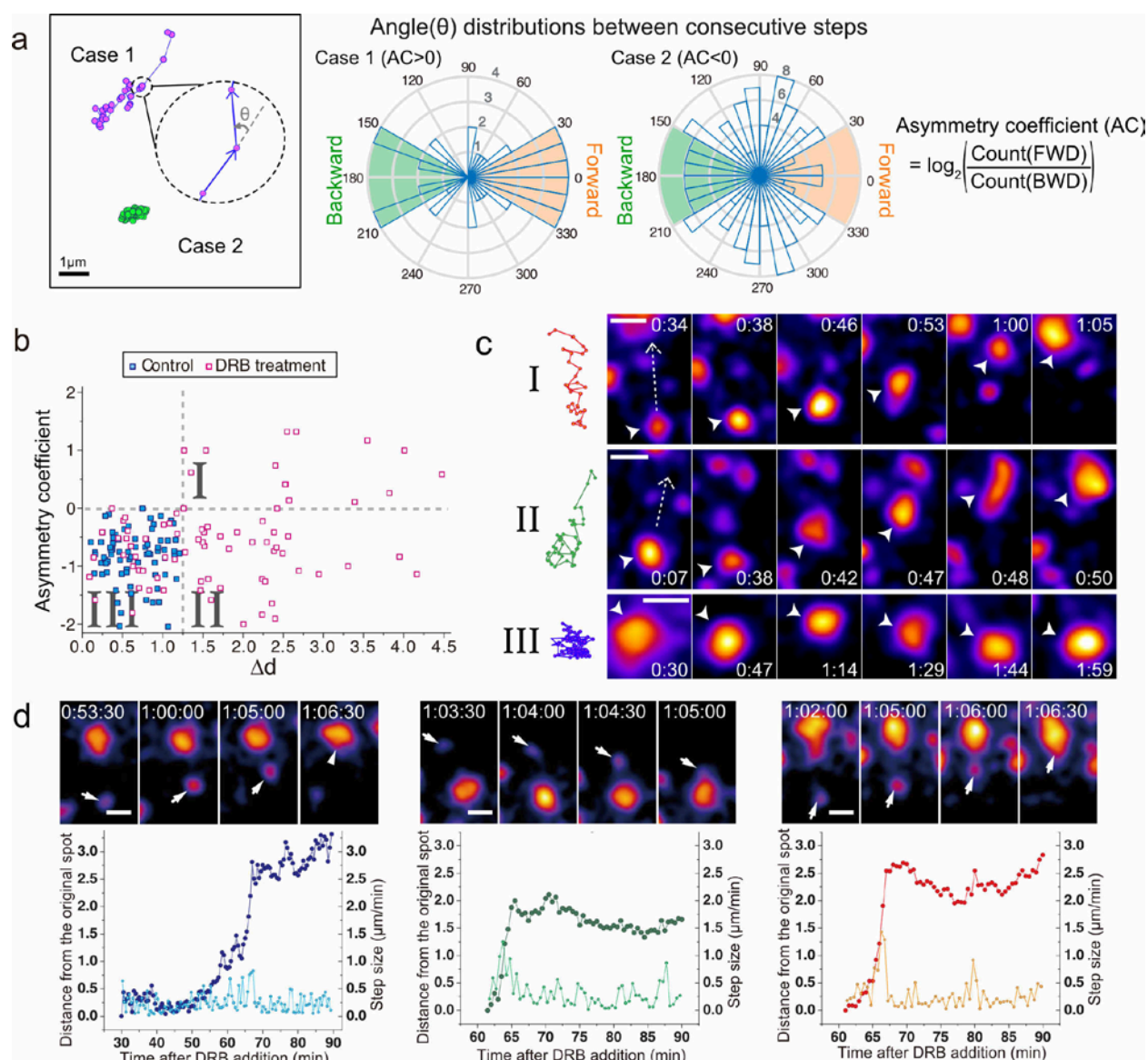
Figure 2. DRB treatment induces long-range, directional speckle movements. a. Analysis of angular distributions for two speckle trajectory examples: (Left) Two speckle trajectories- Case 1 (purple), Case 2 (green). The angle (θ) between every two consecutive steps is calculated (cartoon blowup). (Middle) Histogram distributions of angles for Case 1 (left) compared to Case 2 (right) trajectories. Radius of shaded sectors (blue) shows number of adjacent steps with a given angle. Backward (BWD) steps are defined by angles in green; forward (FWD) steps are defined by angles in orange. Asymmetry coefficients (AC) for Case 1 and Case 2 are negative and positive, respectively, as AC (right) is defined as the log2 ratio of FWD over BWD steps. **b.**

Scatterplot of asymmetry coefficient (AC, y axis) versus net displacement (Δd, x axis) for speckle trajectories from control (blue squares) versus DRB-treated cells (pink squares). 3 trajectory types I-III are defined by their placement within three quadrants (I-III) defined by dotted lines (AC=0; Δd = 1.25). Control cells fall into negative AC and low Δd quadrant (I). n=75 speckles from 10 control cells; n=80 speckles from 10 DRB-treated cells. **c.** Speckle trajectories (left) and corresponding time-lapse images (right) from each of the 3 types I-III in (b). Time (hr:min) is after DRB addition. Scale bars: 1 μm. White dashed arrow marks direction of movement; arrowheads mark moving speckle. (Top) Type I: Forward motion-dominant, long-range directional motion; (Middle) Type II: long-rang directional motion, but fewer forward steps. (Bottom) Type III: Confined speckle motion. See Supplementary Video 1. **d.** Three examples of long-range directed speckle motion. (Top) Time-lapse images. Scale bars: 1 μm. White arrowheads mark speckle that moves. (Bottom) Distance (μm, vivid colors, left y-axis), measured from the starting spot position, and velocities (μm/min, light colors, right y-axis) as a function of time after DRB addition.
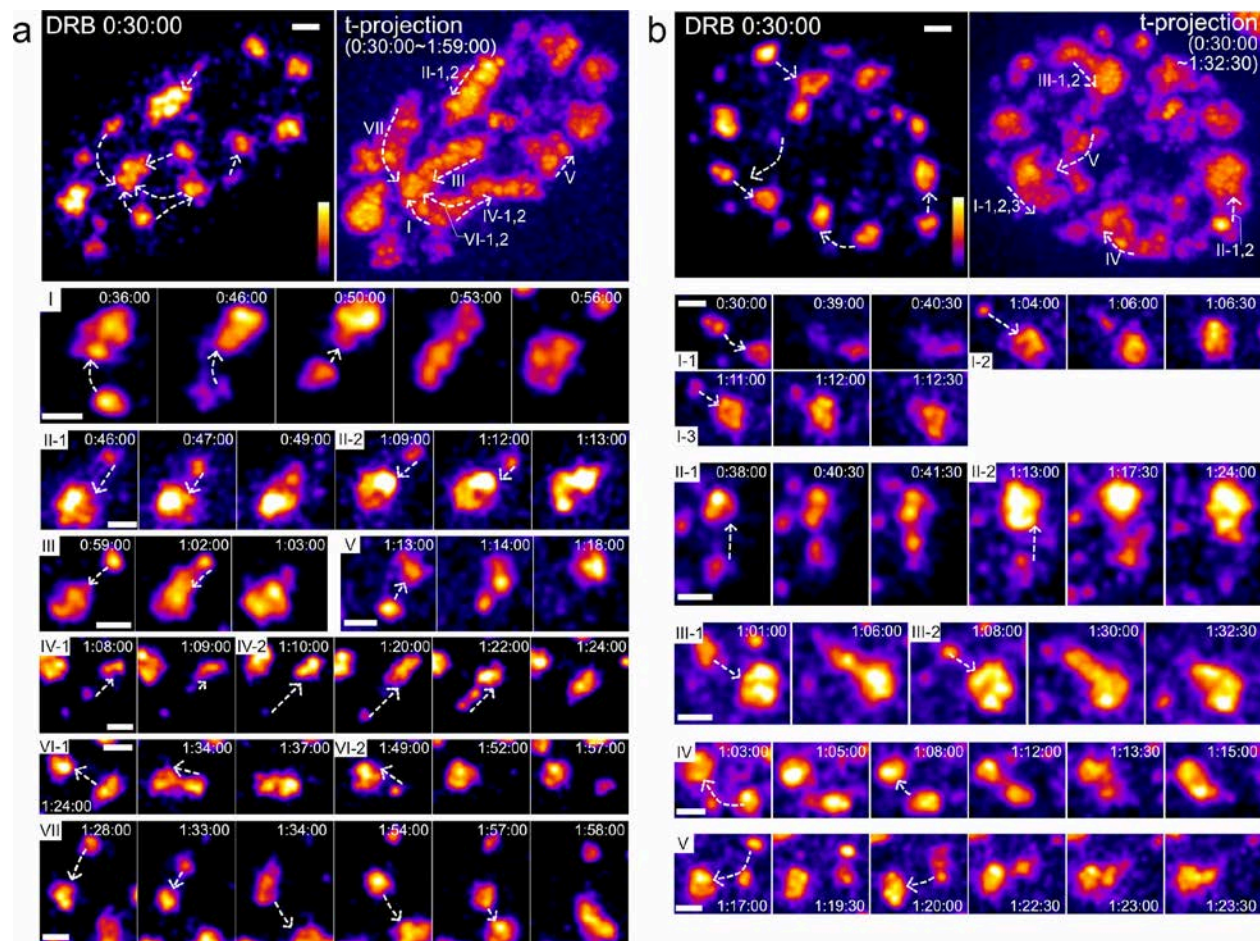
Figure 3. Long-range speckle movements are directed towards other speckles and terminate by speckle fusion. a. Overview of speckle motions in one nucleus (cell clone E8). All images show maximum-intensity 2D projections of optical sections, using pseudo-color intensity scale. Time (hr:min:sec) is after DRB addition. Scale bars: 1 µm. White dashed arrows show direction of speckle movements. (Top left) First time-lapse image taken 30 mins after DRB addition. (Top right) Maximum-intensity projection over all time-lapse 2D images. Roman numerals indicate different regions showing speckle movements, ordered by the time of speckle movements. Some regions show multiple speckles appear and then move. Each of these speckles is tagged by a number following the roman numeral (i.e. II-1,2 shows path of two different speckles moving in region II). (Bottom) Time-lapse images of each speckle movement marked by roman numeral and speckle number. See Supplementary Video 2. **b.** Same as (a) for second nucleus (cell clone D6). See Supplementary Video 3.
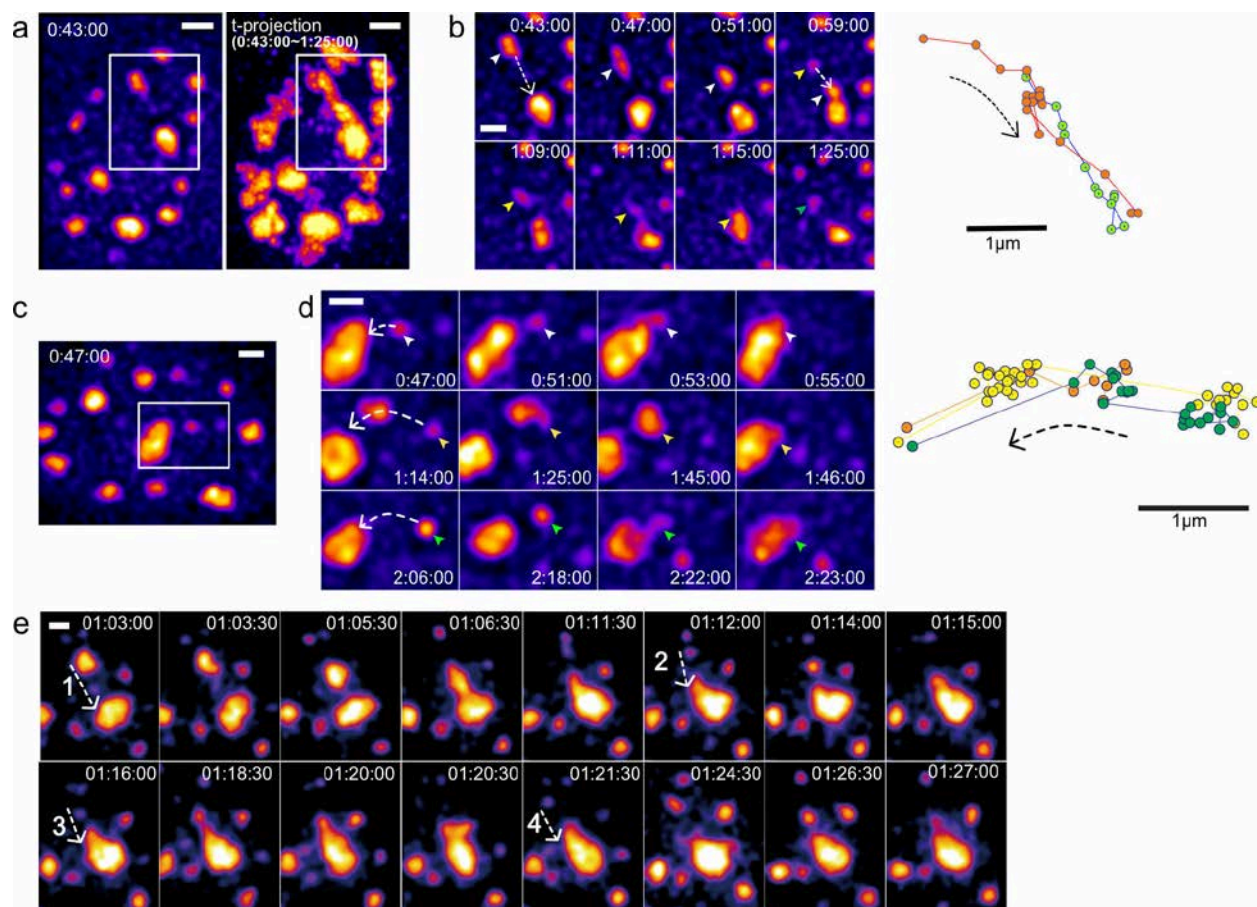
Figure 4. Multiple speckles undergo long-range, directional movements along similar paths: repeated cycles of speckle nucleation, motion, and fusion to same target speckle. 2D images represent 2D maximum-intensity projections of z-stacks. GFP-SON intensities are pseudo-colored to increase dynamic range. Time (hr:min:sec) represents time after DRB addition. Scale bars: 1 μm. **a.** (Left) Image of first cell nucleus 43mins after DRB addition, with boxed region containing repeated long-range speckle motions shown in (b). (Right) Maximum-intensity projection of multiple 2D projected images over time from 43 mins to 1 hr 25 mins. An elongated high intensity "trail" is generated by the time projection of repeated speckle movements. **b.** (Left) Time-lapse images of speckle movements within boxed region in (a). White dotted arrow lines show the direction of speckle movements. First speckle (white arrowheads) moves and merges with target speckle. Second speckle (yellow arrowheads) appears along path followed by first speckle and moves to same target speckle. Green arrowhead marks appearance of third speckle along same path. (Right) Trajectories of first

(brown) and second (green) moving speckles, showing their close overlap. **c.** Image of second cell nucleus 47 mins after DRB addition, with boxed region containing repeated speckle motions shown in (d). **d.** (Left) Time-lapse images of speckle movements within boxed region in (c). White dotted arrow lines show the direction of speckle movements. White, yellow, green arrowheads point to 3 different speckles that move over similar paths. (Right) Trajectories of these 3 speckles showing their close overlap. Second (yellow) and third speckles (green) nucleate at similar location but at different times. **e.** An additional example of 4 repeated speckle movements along similar paths. See Supplementary Video 4 for boxed regions shown in b, d, e.
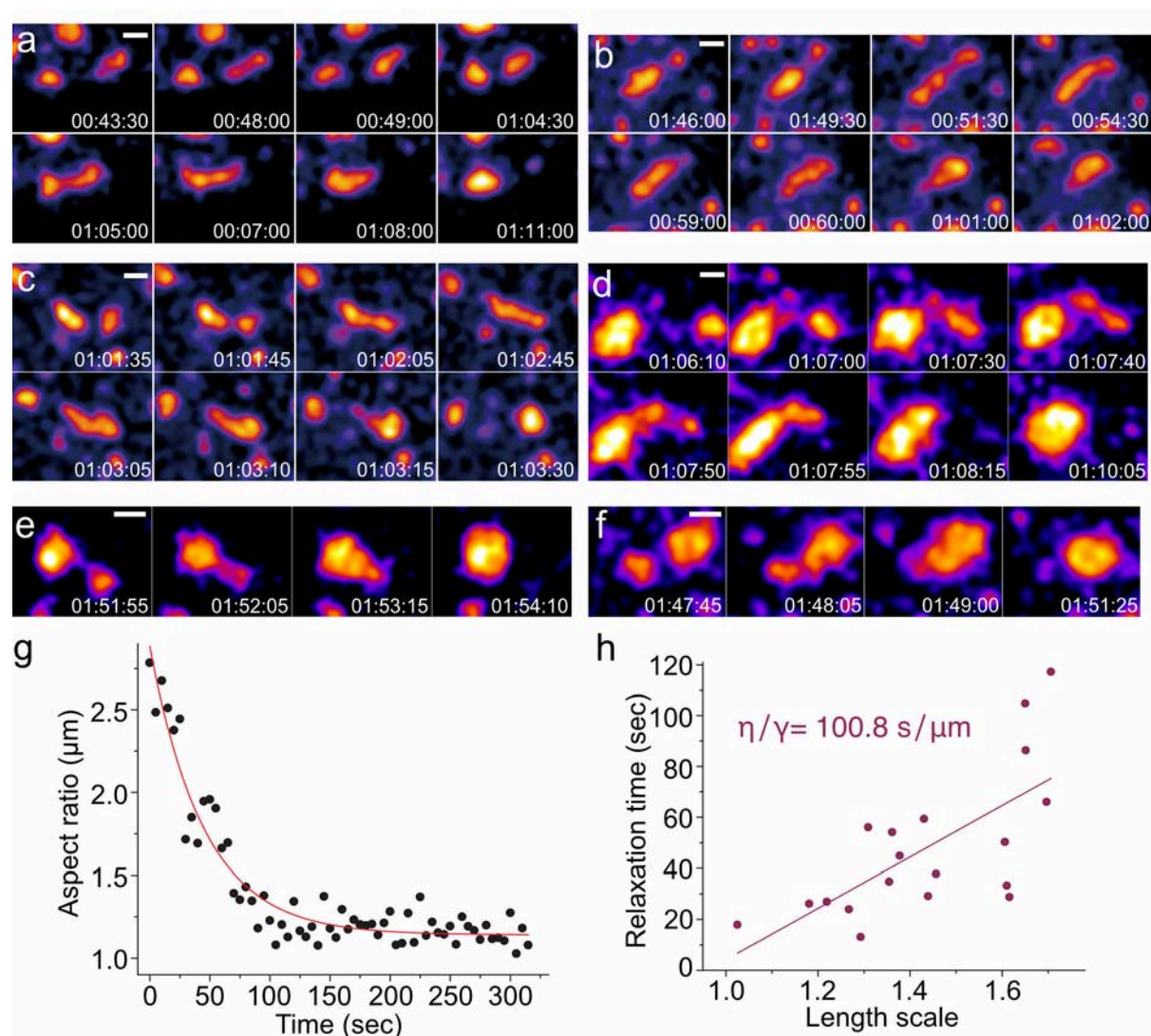
Figure 5. Viscoelastic behaviors of nuclear speckles. SON-GFP images represent maximum intensity 2D projections of 3D image stacks. Time (hr:min:sec) is after DRB treatment. Scale bars: 1 um. **a.** "Inch-worm"-like motion: A nuclear speckle repeats cycles of elongation and translocation until it fuses with another speckle located ~3 µm away from starting position of first speckle. **b-d.** reptation motion**:** A speckle elongates towards and then fuses with another speckle prior to speckle rounding. **e-f.** Two examples of most commonly observed speckle fusion. **g.** Plot of the aspect ratio versus time for two speckles fusing with each other. The Aspect Ratio is defined as the ratio of the long axis (l_{long}) to short axis (l_{short}) lengths of the ellipse approximating the morphology of the fusing speckles. Fitting this plot to a single exponential decay curve yields an exponential decay constant corresponding to the relaxation time of the speckle fusion. In this example, the relaxation time was calculated as 44.9 sec. **h.**

Plot of relaxation time versus length scale for multiple speckle fusion events (N=19). The slope of this linear fit of relaxation time versus length scale, corresponds to the inverse capillary velocity, equal to the ratio of viscosity to surface tension (η/γ). The measured inverse capillary velocity from this plot = 100.8 s/μm.
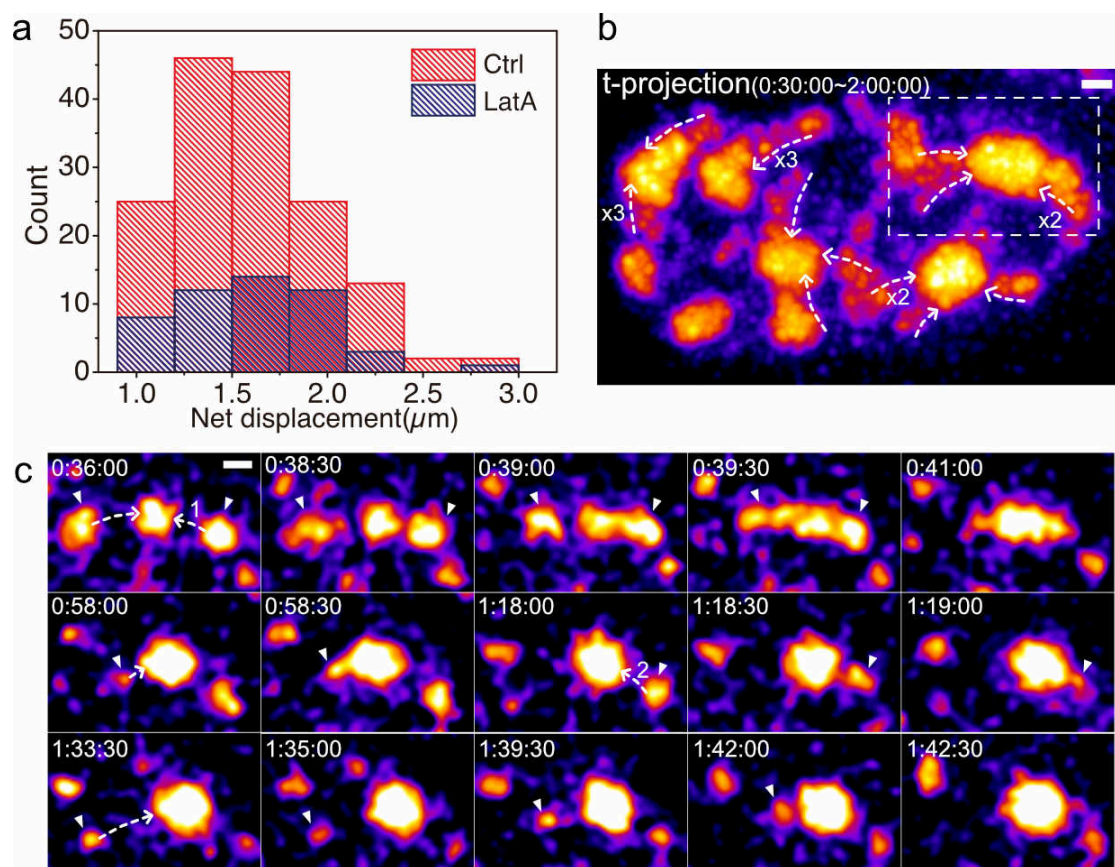
Figure 6. Long-range speckle motion does not require polymerized actin. **a.** Histogram of speckle net displacements after DRB addition with or without latA. LatA treatment decreases the frequency of long-range speckle motion, but not the length distribution of their net displacements. **b.** Maximum-intensity projection over time (t-projection) of GFP-SON nuclear 2D projections from 30 mins to 2 hrs after DRB and latA treatment. This t-projection shows curvilinear paths of long-range speckle motions which terminate at another speckle. White dotted lines indicate direction of speckle motions. Numbers show the number of speckles that move along the direction of the arrow over time (no number for one speckle). Time (hr:min:sec) represents time after DRB addition. Scale bar: 1 µm. See Supplementary Video 5. **c.** Time-lapse images from the boxed region in (b). Arrowheads point to moving speckles, and dotted lines indicate direction of speckle movements. The number on the dotted line distinguishes different speckles that move on the same path. Time (hr:min:sec) represents time after DRB addition . Scale bar: 1 µm.
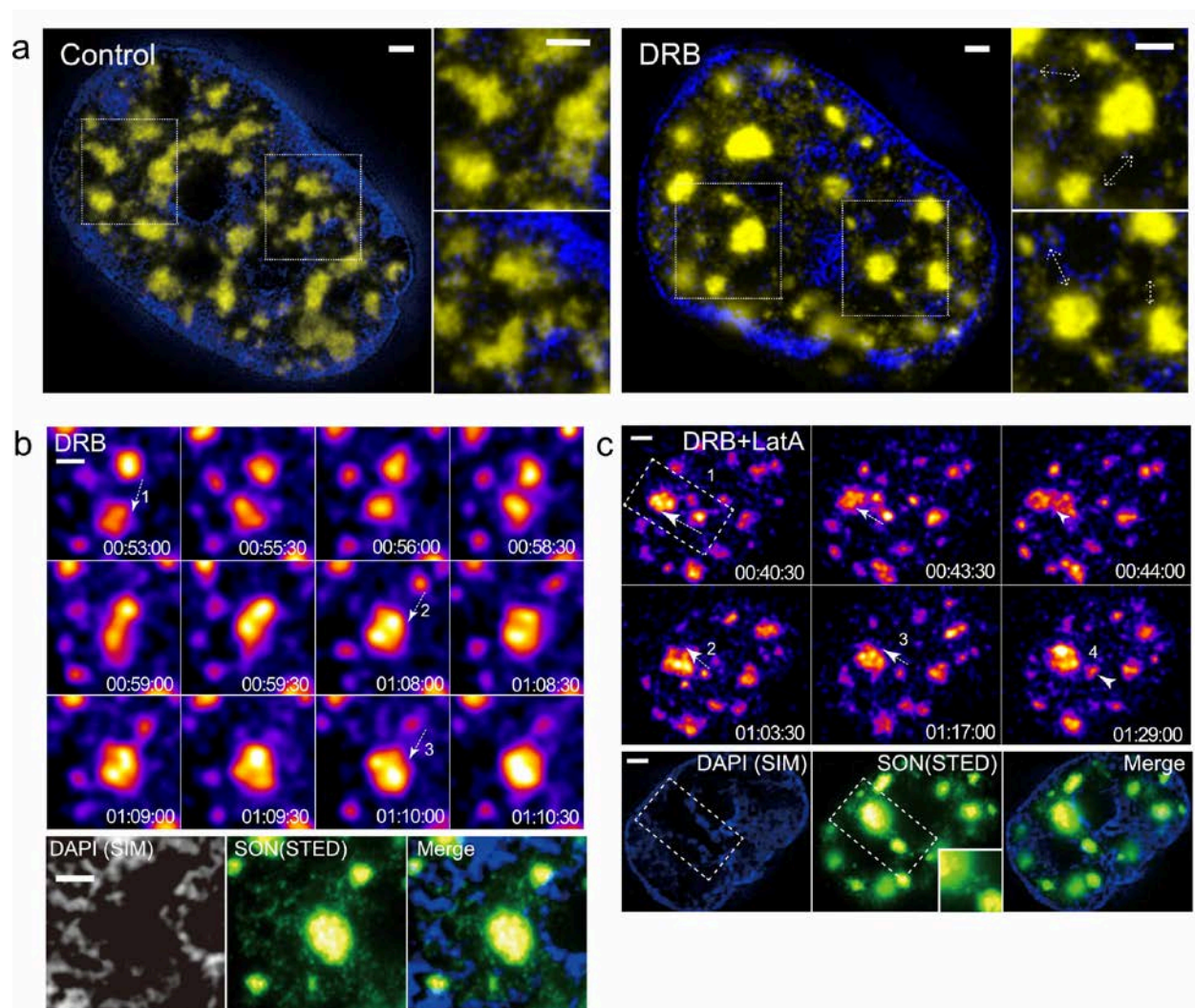
Figure 7. Repeated nuclear speckle motions occur within DAPI-depleted regions enriched in SON granules. Scale bars: 1 μm. **a.** Correlative SIM (DAPI, blue) and STED (SON, yellow) images of single optical sections, showing heterogeneous distribution of nuclear speckles and SON granules in DAPI-poor regions before (left) and after (right) DRB treatment. Regions of interest are marked with dotted boxes and shown enlarged in panels to right of nuclear images. Dotted arrows (right panels, right side) are drawn adjacent to local accumulations of SON granules running between two nearby nuclear speckles. **b.** Correlation between the path of repeated speckle motions, DAPI-depleted region, and local concentration of SON granules in DRB-treated cell. (Top) Time-lapse images of repeated speckle motions. Each speckle motion is marked by arrow and number. Time (hr:min:sec) is after DRB addition. See Supplementary Video 6. (Bottom) Correlative super-resolution images after fixation in region of repeated speckle

movements(Top) occurred in DAPI-depleted region (left) enriched in SON granules (middle). Merged image (right). **c.** Same as (b) but for latA and DRB-treated cell. See Supplementary Video 7.
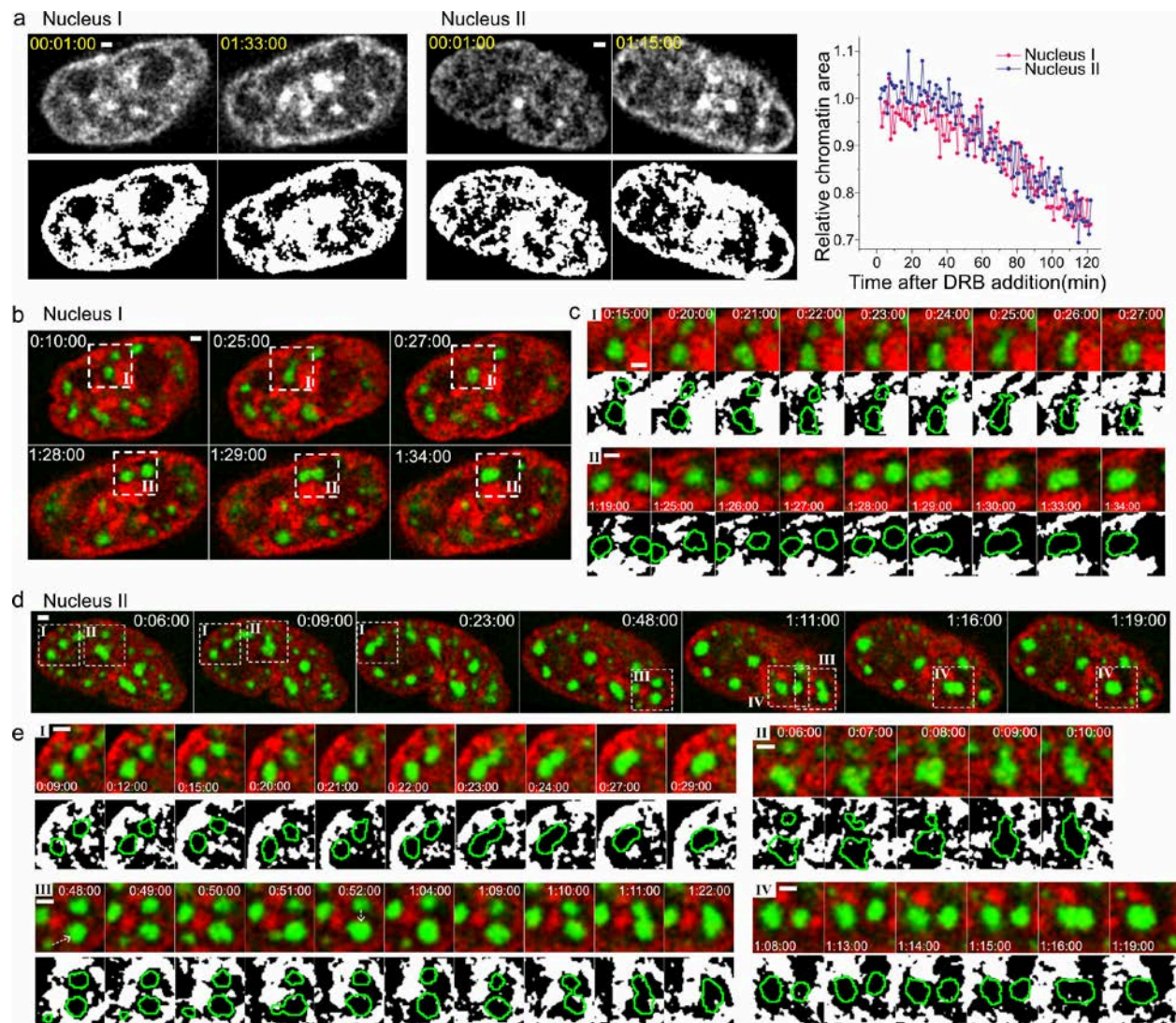
Figure 8. Speckle motions are spatially limited by chromatin structure. All images show single optical sections. Time (hr:min:sec) is after DRB addition. Scale bars: 1 μm. **a.** Chromatin compaction over time after DRB addition. (Left, Middle) Gray-scale (top) and binary (bottom) images of chromatin (SiR-Hoechst) in nucleus I (left) and nucleus II (middle) at indicated time points. (Right) Change in relative chromatin area (y) over time after DRB addition (x). **b.** Time-lapse images of nucleus I showing speckle (GFP-SON, green) motions and fusion following loss of chromatin (SiR-Hoechst, red) between the speckles that fuse. See Supplementary Video 8. Regions of interest (ROI) I and II marked by dashed lines are shown enlarged in (c). **c.** (Top row for ROI I and II) Time-lapse images show speckle-merging events occurred after depletion of chromatin in space between speckles. (Bottom row for ROI I and II) Binary images of

thresholded SiR-Hoechst staining (white) relative to speckle boundaries (green lines). **d**. Same as (b) for nucleus II. See Supplementary Video 9. Nucleus II contains four ROI (I-IV). **e.** Same as (c) for nucleus II.

Supplementary Videos:

Video 1. Speckle movements from trajectory types I-III in live CHO cell after DRB treatment.
Corresponds to Figure 2C. Movie represents maximum intensity 2D projection of 3D image stack for each time point. Time (hr:min) after DRB addition and scale bar(1µm) are stamped on the movie.

Video 2. Long-range movement and fusion of nuclear speckles in live CHO cell after DRB treatment.
Corresponds to Figure 3A. Movie represents maximum intensity 2D projection of 3D image stack for each time point. Time (hr:min:sec) after DRB addition and scale bar are stamped on the movie.

Video 3. Long-range movement and fusion of nuclear speckles in live CHO cell after DRB treatment.
Corresponds to Figure 3B. Movie represents maximum intensity 2D projection of 3D image stack for each time point. Time (hr:min:sec) after DRB addition and scale bar are stamped on the movie.

Video 4. Repeated long-range directional speckle movements after DRB treatment. Corresponds to Figure 4b, d and e. Each example was found in different cell nucleus. Movie represents maximum intensity 2D projection of 3D image stack for each time point. Time (hr:min:sec) after DRB addition and scale bar(1µm) are stamped on the movie.

Video 5. Long-range movement and fusion of nuclear speckles after latrunculin A and DRB treatment.
Corresponds to Figure 5. Movie represents maximum intensity 2D projection of 3D image stack for each time point. Time(hr:min:sec) after DRB addition and scale bar are stamped on the movies.

Video 6. Repeated speckle movements along similar path and fusions with same target speckle after DRB treatment.
Corresponds to Figure 6B. The local region of interest is marked with box in movie. Correlative STED and SIM images of SON and DNA (DAPI) are shown in Figure 6B following fixation and staining. Movie represents maximum intensity 2D projection of 3D image stack for each time point. Time(hr:min:sec) after DRB addition and scale bar are stamped on the movies.

Video 7. Repeated speckle motions along similar path and fusions with same target speckle after latrunculin A and DRB treatment.
Corresponds to Figure 6C. The local region of interest is in the center of the nucleus. Correlative STED and SIM images of SON and DNA (DAPI) are shown in Figure 6C following fixation and staining. Movie represents maximum intensity 2D projection of 3D image stack for each time point. Time(hr:min:sec) after DRB addition and scale bar are stamped on the movies.

**Video 8. Speckles fuse after chromatin barrier is depleted.**
Corresponds to nucleus I in Figure 7. SiR-Hoechst staining (red) with GFP-SON (green) after DRB treatment. Movie is a single optical section for each time point. Time(hr:min:sec) after DRB addition and scale bar are stamped on the movies.

Video 9. Speckles fuse after chromatin barrier is depleted.
Corresponds to nucleus II in Figure 7. SiR-Hoechst staining (red) with GFP-SON (green) after DRB treatment. Movie is a single optical section for each time point. Time(hr:min:sec) after DRB addition and scale bar are stamped on the movies.
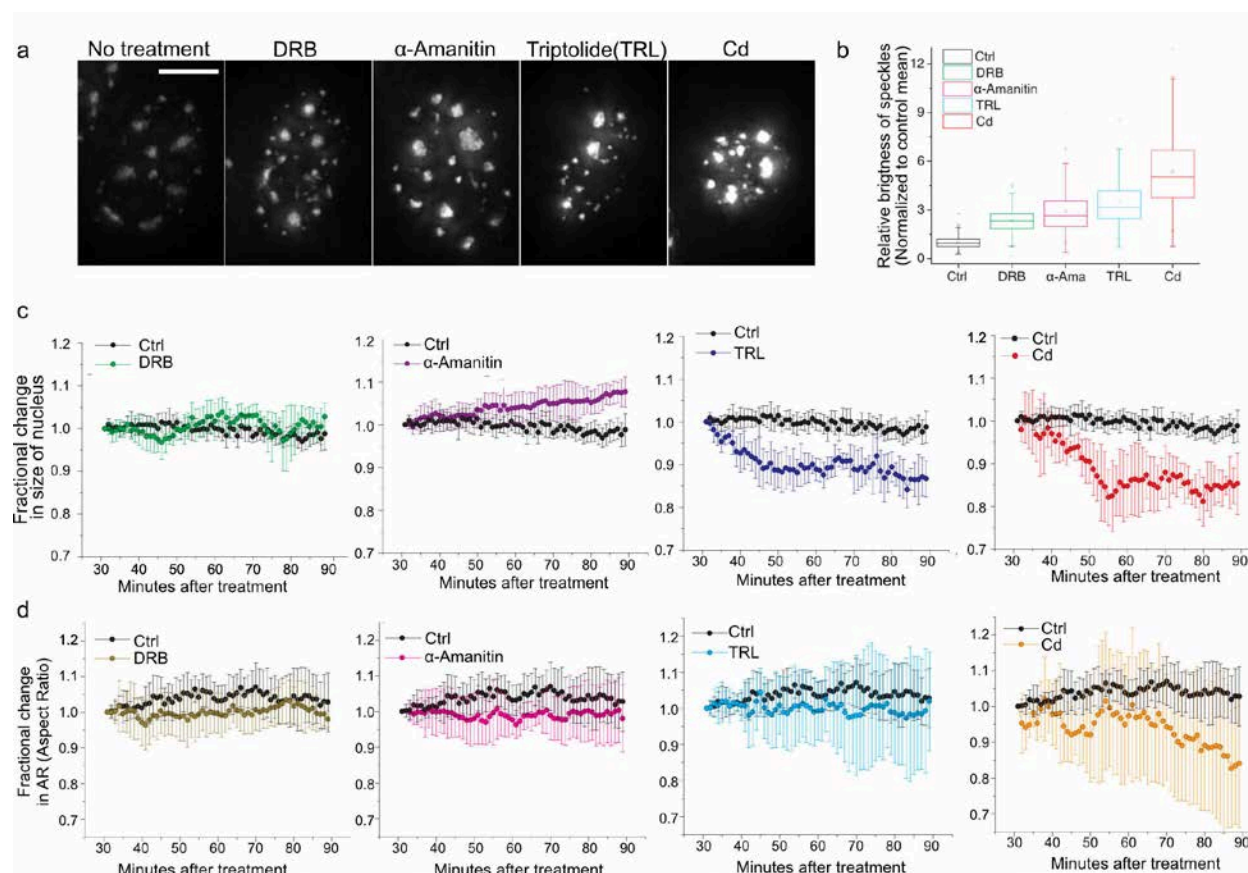
Supplementary Figure. 1. Morphological changes of nuclear speckles and nuclei after treatment with different transcription inhibitors or cadmium (Cd). **a.** Fixed cell images after 2 hr treatment with the indicated chemical. Scale bar: 5um**. b.** Box plots summarizing statistical distribution of relative brightness of individual speckles after treatment with indicated chemical normalized to the mean of speckles in control cells. **c.** Fractional change in the size of nucleus during 1 hr live cell imaging of control (Ctrl, black) or treated cells (Chemical indicated, color). Triptolide (TRL). Error bars represent standard deviations between cell nuclei. **d.** Fractional change in aspect ratio of the nuclear major axis to minor axis during 1 hr live cell imaging. Error bars represent standard deviations between cell nuclei.
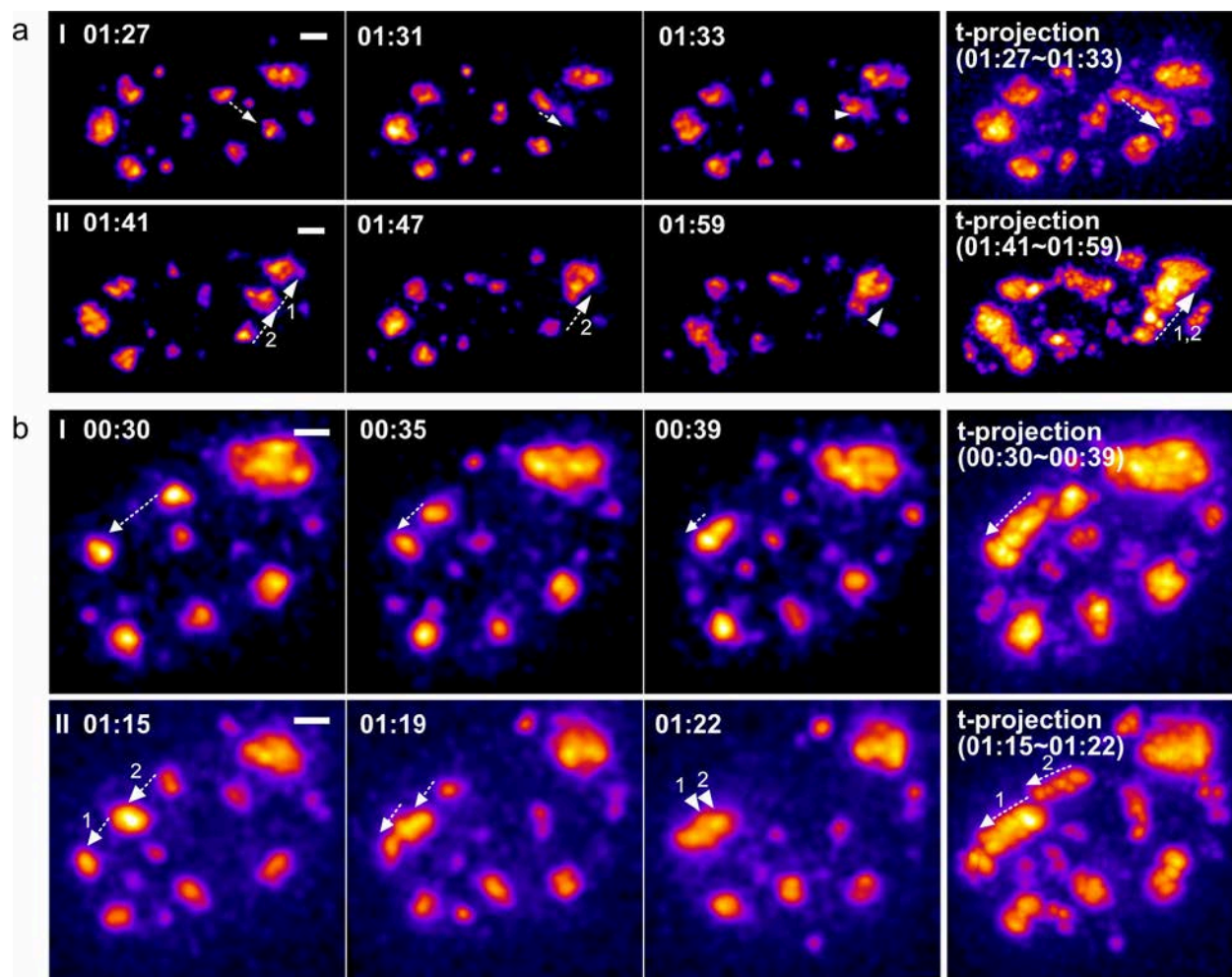
Supplementary Figure. 2. Linear path of long-range (>1μm) directional speckle movements.

SON-GFP images represent maximum intensity 2D projections (left) of 3D image stacks or maximum intensity projections over time (t-projection) of these 2D projections (right). Time (hr:min) is after DRB treatment. Scale bars: 1 μm. **a.** (I,II) Examples of long-range directional speckle movements within one nucleus. (Left) White arrows: direction of each speckle movement. **b.** (I,II) Additional examples from second nucleus.
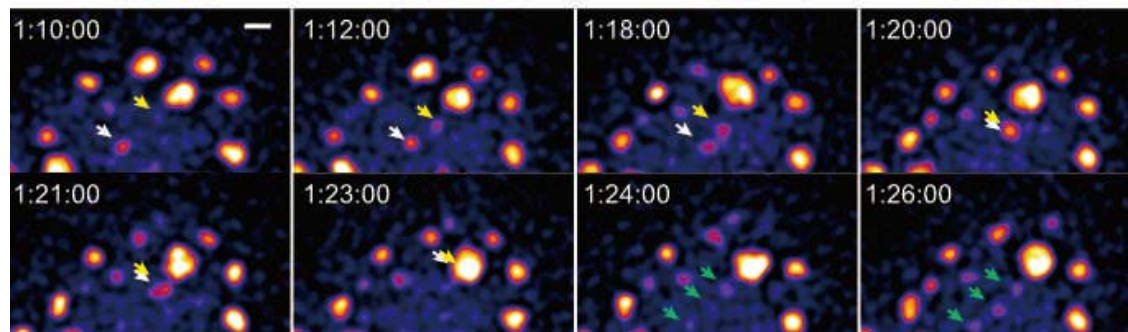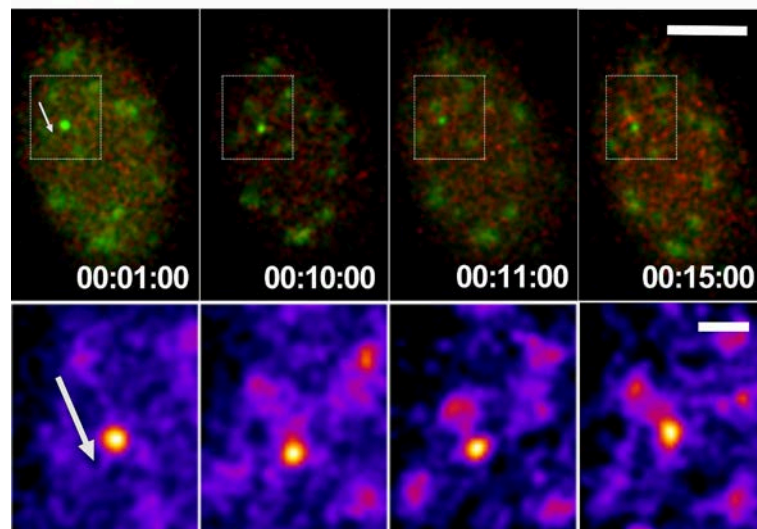
Supplementary Figure 3. Nucleation of speckles along a path followed by a nuclear speckle.
SON-GFP images represent maximum intensity 2D projections of 3D image stacks. Time (hr:min:sec) is after DRB treatment. Scale bar: 1 um. As a first speckle (white arrowhead) moves towards a large, target speckle, a second, small speckle (yellow arrowhead) appears to nucleate at a position on linear path connecting the first and target speckles. The first speckle moves along this linear path, fuses with the second speckle, and then the fused speckle continues along this linear path and fuses with the large target speckle. One minute later, three new small, collinear speckles (green arrowheads) form along this same path.
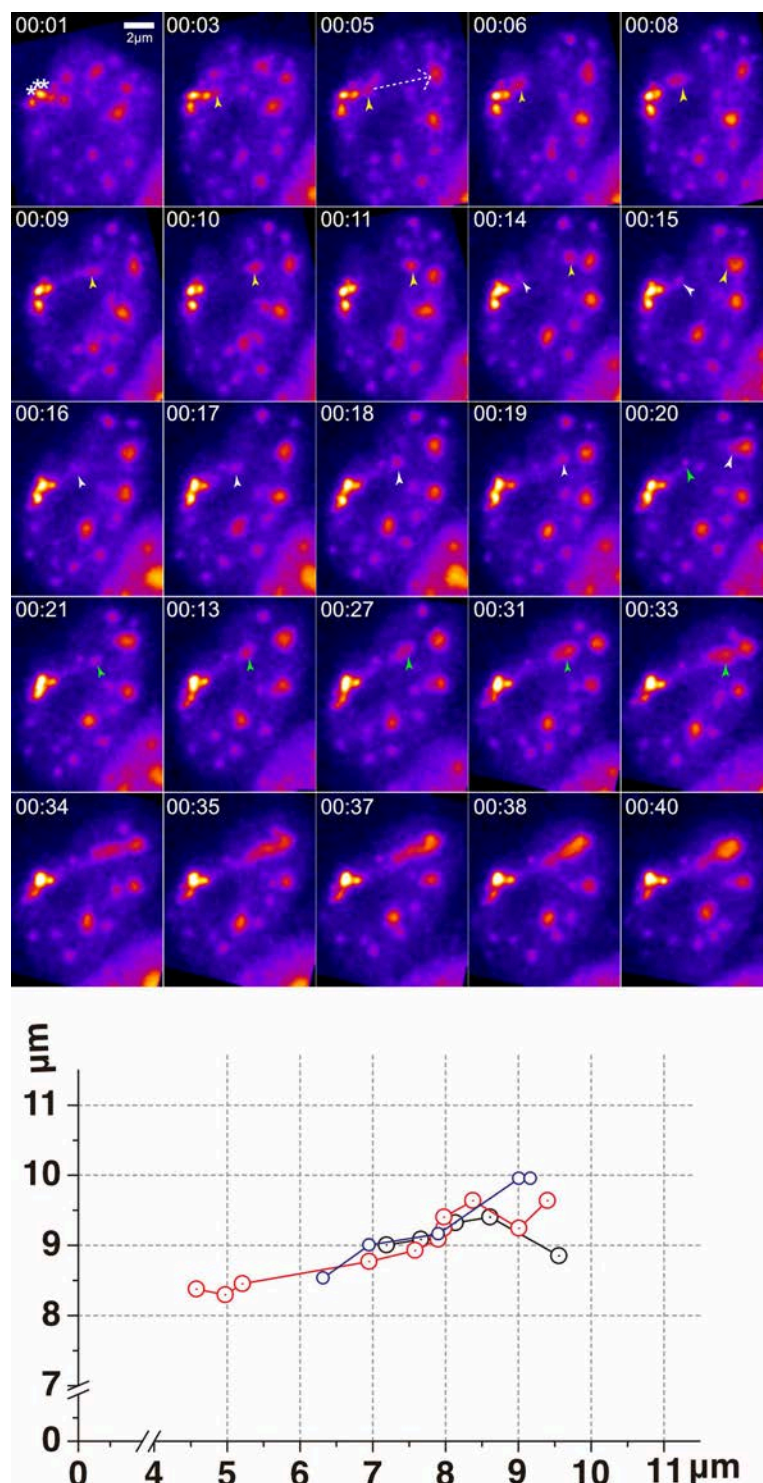
Supplementary Figure 4. Repeated cycles of speckle formation, translocation and fusion. Top: Pseudo-colored GFP images showing SON-GFP (speckles) and GFP-lac repressor (Hsp70 plasmid transgene array) (Khanna et al. 2014) represent maximum intensity 2D projections of 3D image stacks. Time (hr:min) is after heat-shock induction of Hsp70 transgene array. Scale bar: 2 μm.

Nuclear speckles nucleate adjacent to Hsp70 transgene array (brightest spot, marked by asterisks 1min), move along linear path (white dashed arrow, 5 min) to fuse with large target nuclear speckle. Three cycles of speckle nucleation, long-range movement, and fusion to same target speckle are seen. Arrowheads (yellow, white, and green- in order of speckle formation) mark moving speckles. Bottom: Trajectories (x,y) of each long range directional speckle movement.

Supplementary Figure. 5. Nuclear speckle movement towards heat-shock, transcriptionally activated Hsp70BAC transgene occurs along path marked by local GFP-SON accumulation. Top: Speckle movement (white arrow) occurs along a linear path. Images of SON-GFP (speckles, light green) and GFP-lac repressor (Hsp70 transgene, brighter green) and mCherry-MS2-binding protein (red) represent 2D maximum intensity projections of 3D image stacks. Time (hr:min:sec) is after heat-shock induction of Hsp70 transgene. The mCherry-MS2-binding protein stains MS2-tagged transcripts of the Hsp70 transgene. Scale bar: 5μm.

Bottom: Enlarged views of boxed region from top images. Subsequent speckle movement occurs along linear path (white arrow) marked by GFP-SON accumulation at 1:00 min after heat-shock. Pseudo-color display of GFP intensities provides improved dynamic range for visualization. Images were coded with 'Fire' LUT in ImageJ. The brightest spot (yellow) marks the Hsp70 transgene; purple regions are GFP-SON. Scale bar: 1 μm.